Annu. Rev. Nucl. Part. Sci. 1999. 49:341–88

MICROPATTERN GASEOUS DETECTORS

Fabio Sauli
CERN, European Laboratory for Particle Physics, EP Division, CH-1211, Geneva 23, Switzerland; e-mail: fabio.sauli@cern.ch

Archana Sharma
GSI, Gesellschaft für Schwerionenforschung mbH, Darmstadt, Germany; e-mail: archana.sharma@cern.ch

Key Words microstrip, parallel plate counter, gas electron multiplier, radiation detectors, high-rate tracking

■ **Abstract** Introduced in 1988, microstrip gas chambers perform considerably better than classic multiwire detectors. Excellent localization, high rate capability, and good granularity make them attractive for charged-particle tracking at high-luminosity colliders, among other applications. The technology continues to improve; for example, substrates have been developed that prevent charge accumulations. Some problems persist, namely the slow degradation under sustained irradiation (aging) and the serious damage that can result from accidental discharges. New types of detectors aim at improving on these points; the microdot, micromegas, and gas electron multiplier detectors are promising examples. They are generally more reliable and cheaper.

CONTENTS

Performance and Limitations of Multiwire Detectors 342
Microstrip Gas Chambers 343
Basic Structure and Operation 343
Electric Field Configurations 346
Manufacturing Technologies and Choice of the Substrate 348
Optimization of Design and Operation 354
Assembly of Detector Modules 355
Detection and Localization of Charged Particles 357
Two-Dimensional Readout 360
Long-Term Performance: Discharges and Aging 362
Other Developments and Applications 365
Alternative Micro-Anode Structures 367
Microgap and Small-Gap Chambers 367
Microdot Chamber 368
Novel Micropattern Detectors 370
Thin-Gap Parallel-Plate Structures, Micromegas 370

0163-8998/99/1201-0341$08.00

Trenches and Holes, CAT and Micro-CAT 374
The Gas Electron Multiplier 374
Summary and Conclusions 383

PERFORMANCE AND LIMITATIONS OF MULTIWIRE DETECTORS

Introduced in 1968 by Charpak (1) at the European Organization for Nuclear Research (CERN), the multiwire proportional chamber (MWPC) revolutionized the instrumentation of particle physics experiments. Exploiting avalanche multiplication around thin anode wires, the MWPC permits fast detection and localization of small amounts of charge released in a gas by ionizing radiation. Numerous generations of multiwire gaseous devices have been developed from the original progenitor, such as drift, time-projection, time-expansion, and ring-imaging chambers (for exhaustive coverage, see 2–7). Gradually replacing slower tools, multiwire devices of various designs remain major components of detectors for particle physics. Their use has spread into other research fields, including astrophysics, industrial and medical diagnostics, and biology (8, 9). In recognition of his invention, Charpak received the 1992 Nobel Prize for Physics.

Confronted by the increasing demands of particle physics experiments, MWPCs have continuously improved over the years. However, limitations have been reached in rate capability and granularity. Placing and holding the thin anode wires at distances closer than a few millimeters is difficult. Moreover, the electrostatic repulsion between thin anodes causes mechanical instability above a critical wire length, which is less than 10 cm for 1-mm spacing. A more fundamental hindrance is the copious production of positive ions in the avalanches, which are only slowly collected by the electrodes and which generate a build-up of positive space charge that modifies the electric field. As a consequence, the proportional gain of the detectors drops quickly at a radiation flux above $\sim 10^4$ s^{-1} mm^{-2}. To overcome these mechanical limitations, gluing the wires to insulating supports was proposed (10), followed over the years by several, often undocumented efforts. The microgap wire chamber is a recent variation on the theme (11). These devices are difficult to use, and their success has been limited because the contact with insulators and glues introduces nonuniform operation.

In 1988, Oed (12) at the Institut Laue-Langevin (ILL) in Grenoble introduced a novel concept: the microstrip gas chamber (MSGC). It consists of a set of tiny metal strips engraved on a thin insulating substrate; these strips are alternately connected as anodes and cathodes. They rely on the same processes of avalanche multiplication as do the multiwire devices. The photolithography used in its manufacturing permits reduction of the electrode spacing by at least an order of magnitude, correspondingly improving the multi-hit capability. Moreover, the fast collection of most positive ions by the nearby cathode strips reduces space-charge buildup and greatly increases rate capability. Introduced coincidentally with the first projects

at high-luminosity colliders, MSGCs filled a gap between the performing but expensive solid-state strip detectors and the cheap but rate-limited traditional gas devices. Intensively developed by many research groups, MSGCs are now components in high-rate tracking systems for major experiments. HERA-B at DESY uses several hundred MSGC plates, measuring 30 cm on the side. The compact magnetic spectrometer (CMS) detector, under construction for the Large Hadron Collider (LHC) at CERN, will deploy around 16,000 MSGC modules in arrays covering a sensitive volume of tens of cubic meters.

Despite their impressive performance, detailed studies of long-term behavior at high rates have revealed possible weaknesses of the MSGC technology. Polymerization processes, occurring in the gas under sustained avalanche conditions, result in the deposition of thin insulating layers on the electrodes and affect the device performance. Discharges caused by imperfections in the photolithography, or triggered by abnormally large energy losses, can permanently damage the thin electrodes. In the effort to improve performance and reliability, alternative detector concepts have emerged recently. Among these new devices, the compteur à trous (CAT) (13) makes use of the avalanche multiplication in narrow holes. The micromegas (14) exploits high-gain properties of narrow-gap parallel plate multiplication. The microdot (15), a matrix of individual circular counters laid on a substrate, probably represents the ultimate gaseous pixel detector. The most recent device, the gas electron multiplier (GEM) (16), has the unique feature of permitting the sharing of the overall gain necessary for detection in a cascade of elements, each operated below the critical voltage for discharges, with a large improvement in reliability.

Starting from the original work on microstrip chambers, this review describes the development, major achievements, and unsolved problems. It also summarizes the recent development of several new devices, collectively named micropattern gas detectors, and attempts a critical discussion of their performances and limitations. In view of the large number of papers on the subject (more than 300 were published in recent years), the authors had to make an excruciating selection. The reader can find coverage of the basic physical phenomena underlying the operation of gaseous counters in the cited literature, as well as in numerous textbooks (17–20).

MICROSTRIP GAS CHAMBERS

Basic Structure and Operation

The MSGC consists of a set of thin, parallel metal strips, deposited on an insulating support and alternately connected as anodes and cathodes. Figure 1 shows a close view of the anode ends in one of the first plates developed at ILL (12). The rear side of the support plate can also have a field-defining electrode, the back-plane, which can be either full or segmented to perform two-dimensional localization. Accurate but simple photolithography technologies can achieve a pitch (distance between

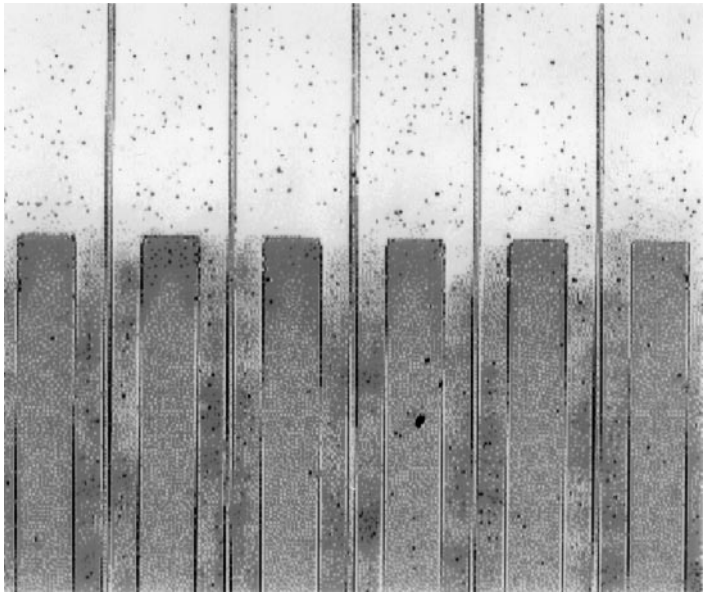

Figure 1 Close view of one of the first microstrip plates developed by Oed at the Institut Laue-Langevin. On an insulating substrate, thin metallic anode strips alternate with wider cathodes; the pitch is 200 μm.

strips) of 100 μm, i.e. improving granularity by an order of magnitude over that of wire chambers. Mounted within a gas vessel, with an upper drift electrode delimiting the sensitive gas volume, the MSGC detects ionization released by radiation. When appropriate potentials are applied to the electrodes, negative with respect to the anode on both drift electrode and cathodes, electrons released in the drift space move toward the strips, start to multiply as they approach the high-field region close to the anodes, and generate detectable signals. For convenience, the readout strips are kept at ground potential, whereas the other strips are powered in groups through protection resistors. Figure 2 shows the electric field equipotentials and field lines in the vicinity of the strips, computed with anodes and back-plane at equal potentials (other configurations are discussed below). All field lines from the drift volume terminate on the anodes, resulting in full electron-collection efficiency. Because of the broad spread of the avalanche, however, a large fraction of the positive ions generated at the anode spills over the field lines connecting to cathodes and is quickly collected. This effect reduces space-charge accumulation and provides a much higher intrinsic rate capability than classic devices can. Moreover, a large fraction of the signal is induced by the rapidly moving ions, resulting in a fast rise time.

In an avalanche, the fast electron collection and the retrograde motion of ions generate negative signals on the anodes. Signals of opposite polarity are induced

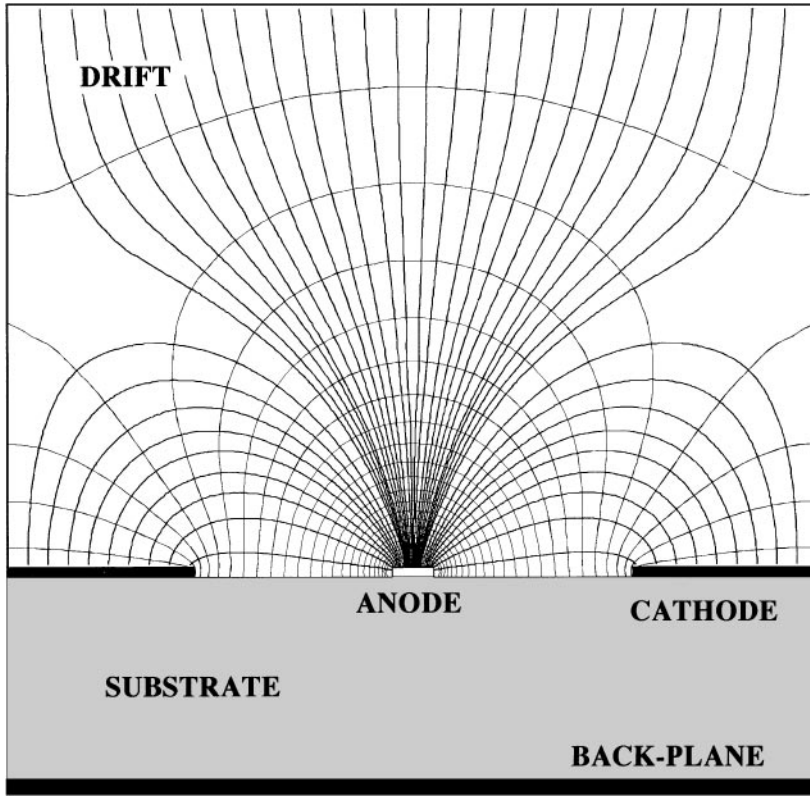

Figure 2 Equipotentials and field lines in the microstrip chamber, computed close to the substrate. The back-plane potential has been selected to prevent field lines entering the dielectric.

on the neighboring cathodes and on the back-plane electrode. Because of mutual capacitance, a fraction of the signal induced on one set of strips is injected into the other (amplitude and extension depend on the grouping scheme), giving the typical charge profile shown in Figure 3.

High gains, very good proportionality, and high resolution have been obtained over a wide range of X-ray energies, essential features for astrophysics applications (21). Along with good position and multitrack resolutions, these characteristics make the MSGC attractive for detection of high-rate, high-multiplicity events. From the beginning, however, various operating instabilities were observed, particularly at high rates. These included time-dependent gain shifts, attributed to substrate polarization and charge accumulation; permanent deterioration (aging) during sustained irradiation; and a tendency to discharge (22, 23). The physical parameters used to manufacture and operate the detectors (substrate material, metal of the strips, type and purity of the gas mixture) appeared to play dominant roles in

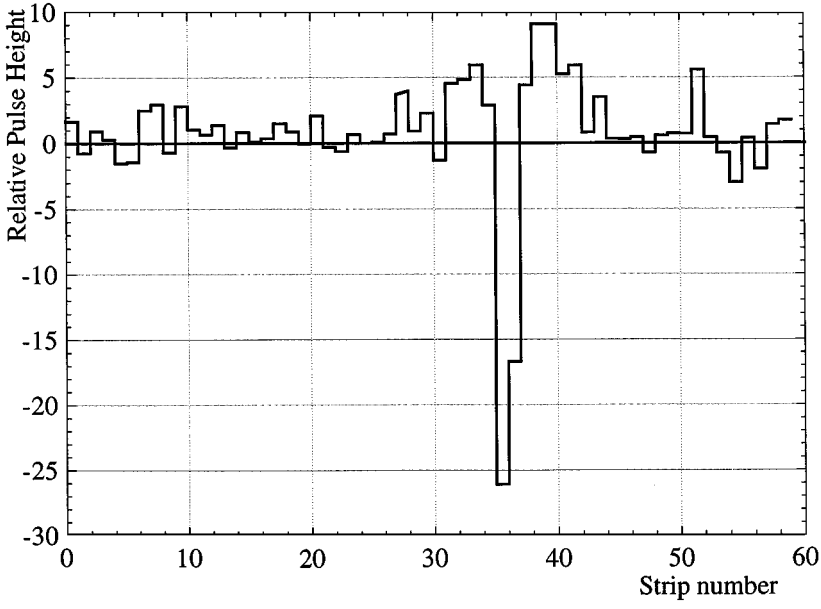

Figure 3 Typical pulse height profile recorded, for a localized avalanche, on adjacent anodes 200 μm apart in a microstrip chamber. The positive overshoot is caused by a signal reinjection from the grouped cathode strips. The width of the distribution, about two strips fwhm (400 μm), determines the multitrack resolution.

determining the medium- and long-term stability. A major effort was undertaken to better understand the MSGCs' operation, to improve their performance, and to increase their lifetime, as well as to reduce manufacturing costs—an essential goal for the technology's extensive use in large systems. A collaboration for the development of MSGCs included more than 40 laboratories worldwide at the peak of its activity. For overviews, the reader is referred to review papers (24–26) and to the proceedings of two dedicated workshops (27, 28).

Electric Field Configurations

The electric field structure in MSGCs has been studied with a variety of tools, from simple analytic approximations to sophisticated models that also account for dynamic charging-up processes (29, 30). Computer codes can be used to map the electric field in complex multielectrode structures and to evaluate drift, diffusion, and multiplication processes (31, 32). The field is constant over most of the sensitive volume, controlled by the drift voltage V_D. It increases toward higher values in the proximity of the strips, where a negative potential V_C applied to the cathodes (anodes being grounded) creates the multiplying field. Because the anode strips are narrower than the cathodes, the field strength can be high enough for electron

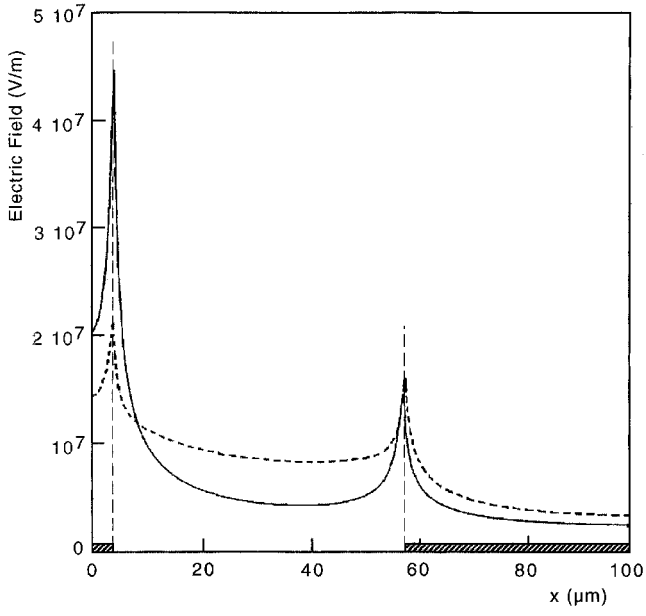

Figure 4 Electric field component parallel to the substrate and close to the surface. The full curve is computed for an insulating substrate, the dashed curve for a substrate with a thin, lower resistivity coating. The origin corresponds to the center of the anode.

multiplication while the field at the surface of the cathode remains below dangerous values. The electric field in the drift region is reduced by the application of the cathode potential, and it is approximately $E_D = (V_C - V_D)/g$, where g is the drift gap.

Computed for the conditions of Figure 2, Figure 4 (solid lines) shows the field strength on a curve just above the substrate surface. The field is uniform over most of the strips' width; the large increase at the ends is responsible for a local increase of gain and for an enhancement of the field emission at the cathode edges.

For insulating substrates, the potential applied to the back electrode, V_B, is important. A back-plane potential close to V_C enhances the multiplying field, permitting larger gains, but results in a number of field lines entering the dielectric (Figure 5). Some of the ions produced in the avalanches reach the substrate and stick to the surface, dynamically changing the field, until a new equilibrium is reached at a reduced gain. Because the equilibrium depends on production and neutralization rates, in general varying over the surface, the operation is unstable. Decreasing V_B toward the potential of the anodes, an optimum condition can be found where no field lines enter the dielectric; this was the case shown in Figure 2. However, because of diffusion of ions during their drift, surface charge accumulation and instabilities can still occur, albeit at higher rates.

Use of substrates with reduced resistivity permits neutralization of the surface charge and extends considerably the rate capability of the MSGC. For thick,

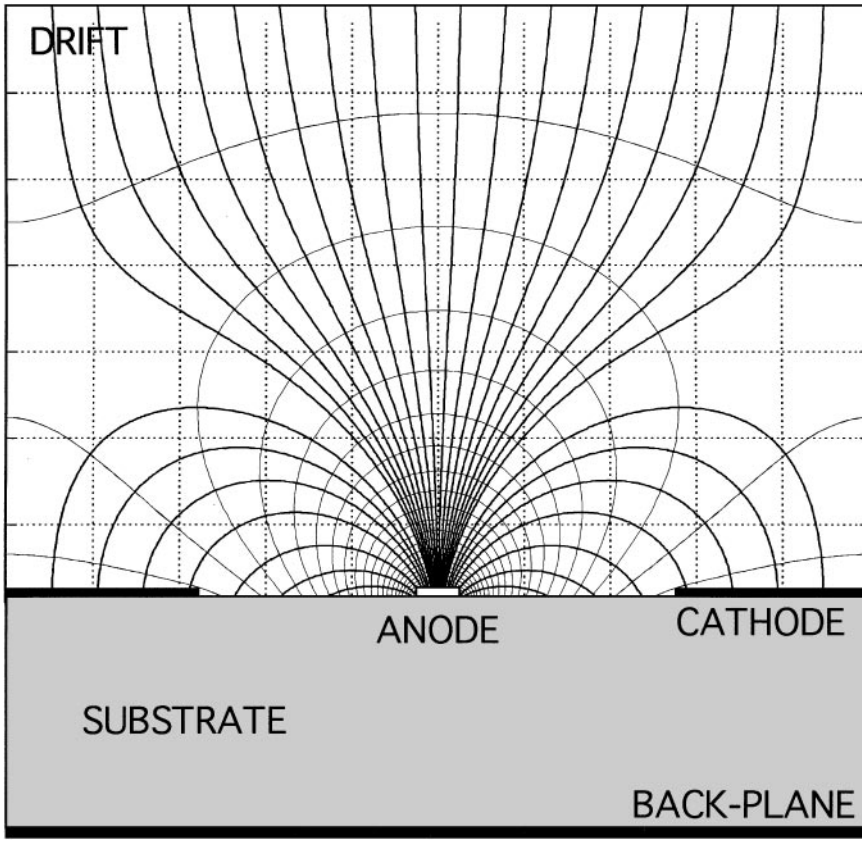

Figure 5 Field lines and equipotentials computed for a back-plane voltage close to the cathode. Field lines enter the dielectric, resulting in a possible accumulation of charge and gain modifications under irradiation.

bulk-conducting supports, the structure of the electric field is identical to that of an insulator's. Such is not the case with a thin conduction layer, where surface currents provide a more uniform field between anodes and cathodes, increasing along the gap and decreasing close to each electrode (Figure 4, dashed curves). This modification of the field entails increasing the voltages to obtain similar gains. A conducting layer also acts as an effective screen for the voltage applied on the back-plane, which can be eliminated altogether, unless it is needed for signal readout.

Manufacturing Technologies and Choice of the Substrate

For detectors to operate properly, the substrate and the metal strips must satisfy strict mechanical and electrical requirements. Adherence of the strips to the

substrate must be excellent in order to prevent the accidental release of conducting fragments (the worst fear for gaseous counters). The surface of the metal itself must be smooth, without field-enhancing roughs, and the edges of the strips must be well defined and preferentially rounded. None of the choices satisfy all requirements; each has its advantages and drawbacks.

Chromium is one of the sturdiest metals used, and it is the only one that can withstand moderate discharges without damage, thanks to its high melting point. However, mechanical stress building up during deposition can induce microcracks and deformations above a thickness of 2000–3000 Å. For thin anodes, the ensuing resistivity of several $k\Omega\ cm^{-1}$ generates a position-dependent attenuation in high-rate applications that require the use of low-impedance amplifiers. With its considerably lower resistivity, gold is a better choice, but the technology for manufacturing gold strips is more difficult and expensive. Moreover, because gold has a low melting point, sparks can seriously damage the strips. Aluminum offers a good compromise between mechanical and electrical characteristics, and it has been adopted for the first, medium-sized experimental setups. Under irradiation, however, aluminum MSGCs suffer considerable degradation of performance with time, even if modest amounts of charge are collected.

Different metals require different methods of deposition on the substrate, often in association: vacuum evaporation, sputtering, electrochemical, or galvanic growth. Except for chromium, which bonds extremely well to glass, most metals are not applied directly but over a previously evaporated, thin adhesion layer, usually nickel and/or chromium. Platinum is often used as migration barrier before gold and silver deposition, to prevent diffusion into the substrate.

Several techniques have been used for manufacturing MSGC plates. In all cases, the final module is a direct or inverted copy of a master pattern, realized with high precision by direct, computer-controlled, laser, or electron-beam ablation. Variations of two methods using conventional, single-mask photolithography have been used industrially to produce the plates.

One method is direct photolithography (Figure 6*a*). The metal-coated substrate is covered with a thin layer of photosensitive resin. A positive mask is overlaid, and exposure to ultraviolet light modifies the open areas, which are chemically removed after curing. Immersion in a solvent (wet etching) or ablation with reactive plasma (dry etching) eliminate the metal from the unprotected areas; the residual resin is then removed and the plate thoroughly cleaned. The technology has been successfully used with chromium and aluminum, and permits manufacture of sizable plates (up to $30 \times 30\ cm^2$) at acceptable costs.

The other method is lift-off (Figure 6*b*). The support is prepared with a thin, metal adhesion layer and coated with the photosensitive resin. Exposure to ultraviolet light through a negative mask, curing, and removal of the exposed areas protects the regions to be freed. The desired metal is uniformly grown by one of the processes mentioned above. Immersion in a solvent removes the polymer, and the overlaying metal peels off. A further short etching step eliminates the adhesion layer in the open regions. Intrinsically more delicate and expensive to implement,

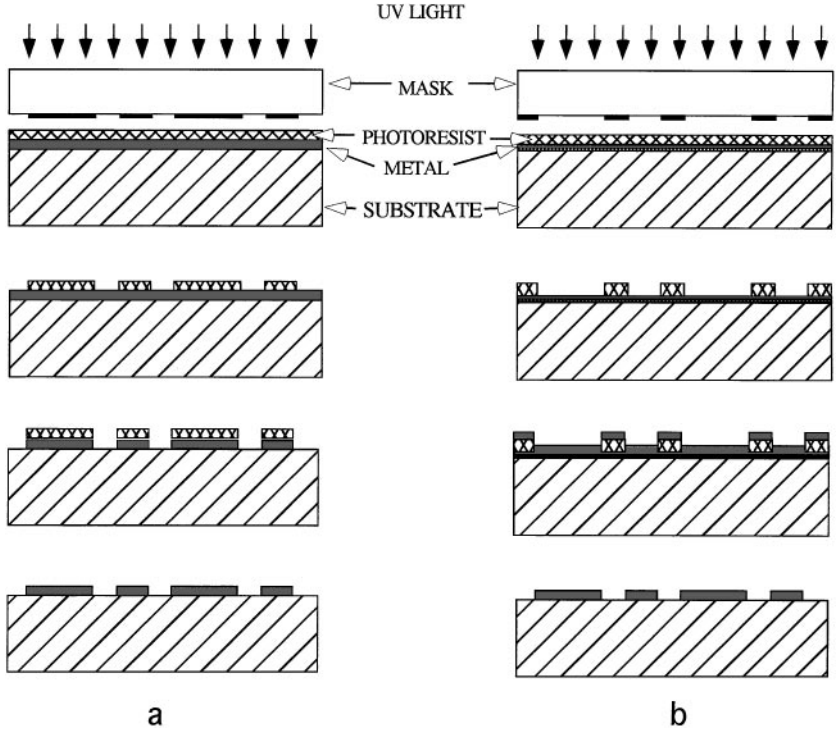

Figure 6 Schematics of two photolithographic methods used for microstrip gas chamber manufacturing: (*a*) direct etching and (*b*) lift-off.

the lift-off technology permits the engraving of patterns in any metal, and even the creation of composite layers of different metals. This method has mainly been used to manufacture MSGCs with gold and aluminum strips.

Other, more sophisticated methods using microelectronics technologies with multiple masks permit the realization of more complex patterns, including insulating layers between electrodes (33). More expensive, and size-limited by current silicon-wafer technology, they have been used mainly for prototyping purposes.

Excellent surface quality, good metal adhesion, and high dielectric rigidity are particularly important for reproducible and stable operation of the detectors. Some applications also demand a light, thin substrate to decrease multiple scattering and photon conversions. The requirements are met by commercially available glasses, such as the borosilicate DESAG D-263 and the alkali-free AF-45.[1] Other rigid substrates have been used: quartz, silicon, ceramics, sapphire, and flexible thin-foil polymers. Most insulators with good surface quality have very high resistivity, above 10^{16} Ωcm. It was recognized early on that this could generate instabilities

[1]Deutsche Spezialglas AG, Grünenplan (Germany).

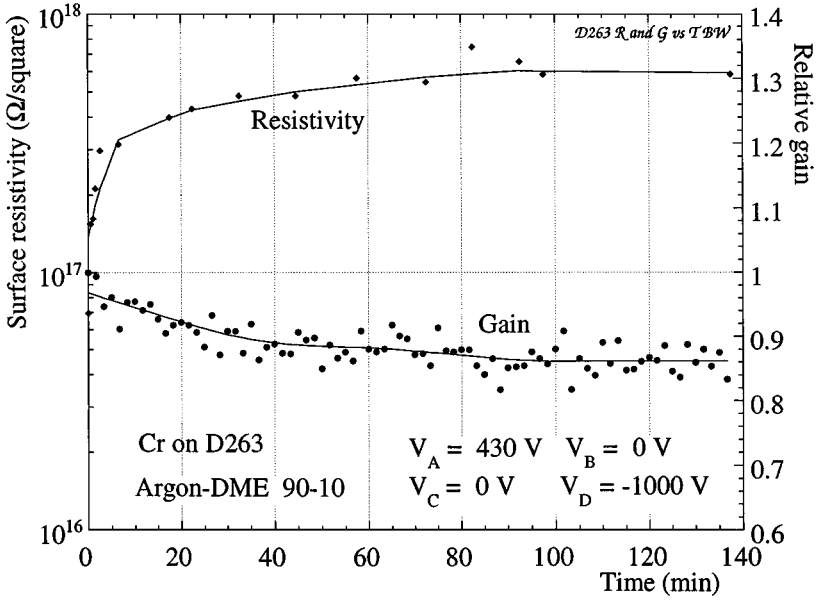

Figure 7 Initial gain variation of gain and resistivity as a function of time from the application of voltage for a plate made on insulating borosilicate glass substrate. V_A, V_B, V_C, and V_D are the anode, back-plane, cathode, and drift potentials, respectively.

owing to local charge redistribution. A fine tuning of the back-plane potential, to minimize the field lines entering the dielectric, and a high value of the drift field permit reasonably stable operation at moderate rates. In most cases, however, a substantial increase of resistivity with time after the application of voltage, accompanied by a decrease of gain (Figure 7) and a rate-dependent gain shift (Figure 8), has been observed (22, 23, 34–36). The effects are attributed to a dynamic modification of the electric field following the application of voltage and to substrate polarization, internal rearrangements of the charge carriers, and surface charge accumulation.

Thermal treatments, either voluntary or as part of the manufacturing process, may alter the surface conductivity and can lead to inconsistent results. This appears to be particularly associated with wet-etching processes (23). Also, since alkali ions are very mobile in glass at high temperature, internal redistribution may occur if the plates are heated for cleaning. When silver electrodes are used, an enhancement of conductivity, imputed to the diffusion of ions into the glass, has been found to improve the stability of operation (37). However, depletion of the metal from the strips has been observed, making this solution unsuitable for long-term operation.

Use of a substrate with lower resistivity and electron conduction eliminates most of the above-mentioned problems. Specialty glasses with resistivity in the range 10^9–10^{12} Ωcm, somewhat inaccurately called semiconducting, have been

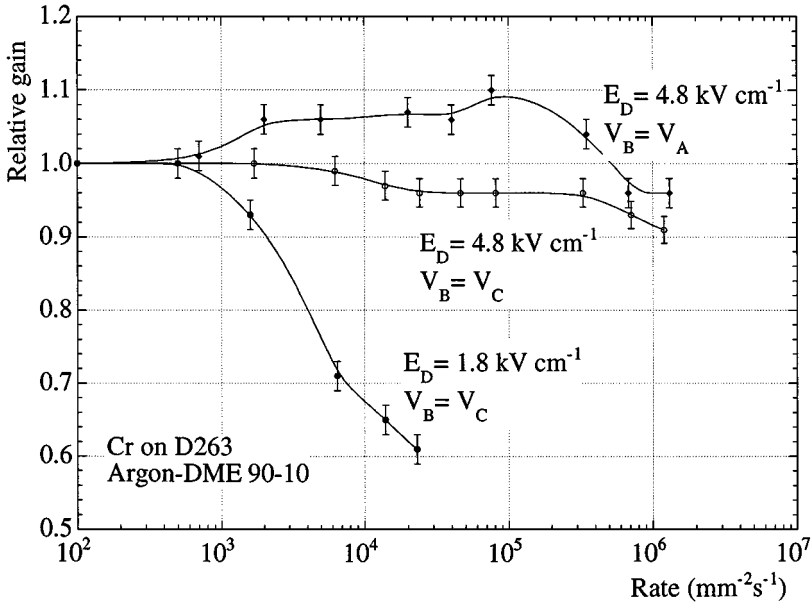

Figure 8 Relative gain as a function of irradiation rate, measured on a microstrip made on borosilicate glass. The performance depends strongly on the applied voltages. E_D is the drift field; V_B and V_C are the back-plane and cathode potentials.

developed. They are often referred to as Pestov glasses after their principal developer (38); some are commercially available (5-8900[2]). MSGCs manufactured on semiconducting glass have demonstrated excellent high-rate performance and long-term stability (23, 39–44), as illustrated in Figure 9 (40). For a glass with resistivity of 10^9 Ωcm, no gain drop is observed up to an X-ray flux of 1 MHz mm^{-2}. Because the leakage current increases with the conductivity and is an intrinsic source of noise, there is no advantage in reducing the resistivity below the value imposed by the rate requirement.

Though promising, bulk-conducting glass is expensive and fragile, particularly in thin layers. Similar characteristics can be obtained reducing only the surface resistivity to equivalent values, between 10^{14} and 10^{15} Ω/square. Several methods of conditioning insulating substrates have been explored to obtain values in this range. Early tests were performed with phosphor and boron implantation in quartz and silicon oxide (21, 45, 46). Some doubts exist, however, about the long-term stability of the implants, since most ions have good mobility in amorphous glass.

Deposition of an electron-conducting layer over the insulating support is a simpler technique to control surface resistivity. Thin layers of lead silicate with the desired values of resistivity have been deposited by reactive magnetron sputtering

[2]Schott Glass Technologies, Dureya, PA (United States).

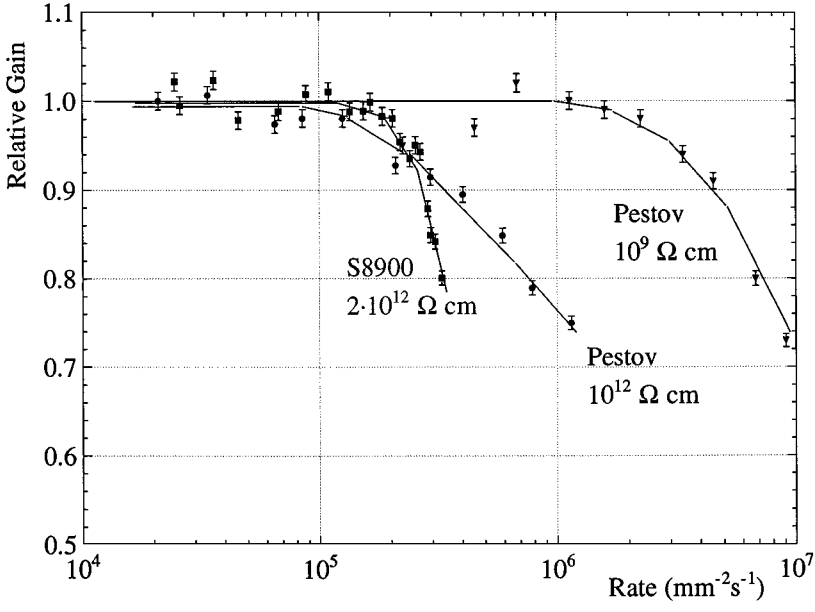

Figure 9 Relative gain as a function of irradiation rate for microstrip chamber plates manufactured on electron-conducting glass of three different resistivities. For 10^9 Ωcm, the gain remains constant up to 10^6 counts $mm^{-2}\,s^{-1}$.

(47, 48) and tested successfully on MSGC plates (49). Using a semiconducting glass target, a conductive layer can be directly sputtered over thin substrates (50, 51). Good uniformity over large areas is possible by means of chemical vapor deposition of diamond-like carbon layers, chemically treated to provide the required resistivity.[3] Detectors made with this technology have been extensively tested and appear to be uniform and stable over a wide range of resistivity (52–55). Figure 10 shows an example of gain measured as a function of rate for MSGC plates built on a diamond-like coated substrate. Using a similar deposition process, several hundred large (30×30 cm^2), thin glass plates have been coated to serve as substrate for the MSGCs built for the HERA-B experiment at DESY (56). Most semiconducting layers, though stable at room temperature, evolve into higher resistivity at temperatures above 100–150°C, particularly in the presence of nitrogen (54), prohibiting post-processing that requires high temperatures, such as baking and polyimide passivation.

Other technologies for surface-resistivity reduction have been studied, such as ion-beam sputtering of amorphous hydrogenated silicon, carbon, and silicon carbide (57–59). Encouraging results have been obtained with thin layers of aluminum nitride (60).

[3]SURMET Co., Burlington, MA (United States).

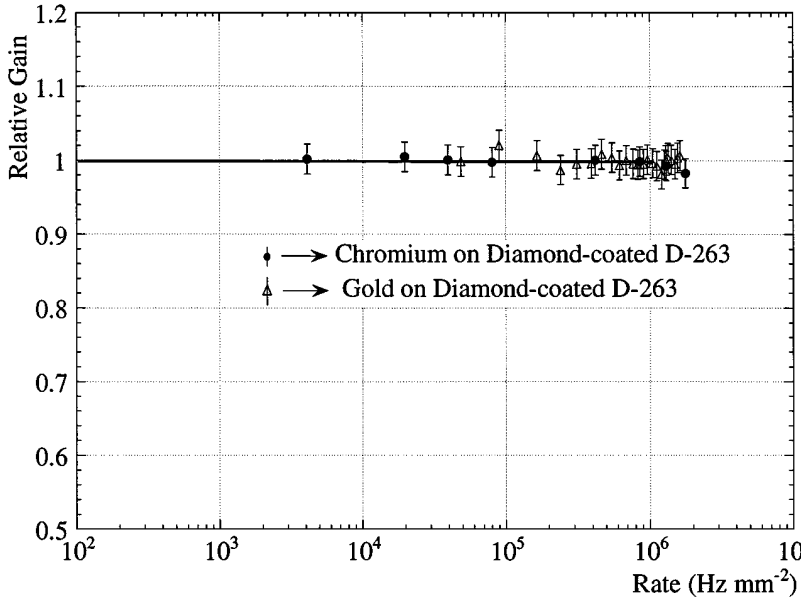

Figure 10 Relative gain as a function of rate for two microstrip chamber plates manufactured with chromium and gold strips, respectively, on glass coated with a thin, low-resistivity, diamond-like carbon layer.

In all described methods of surface conditioning, the insulator is coated before metallization and patterning. Poor adherence of the metal and local imperfections caused by uneven deposition or dust inclusions can create problems. Covering a completed MSGC structure with a thin resistive layer (overcoating) can reduce these problems. Promising results have been obtained using thin metallic layers, such as nickel (61), copper and germanium (62), or lead oxide and doped polymers (49). However, systematic degradation of structures subjected to long-term irradiation has been reported, discouraging the use of the overcoating technology for high-rate applications (63).

Thin polymer foils have also been used as substrates. Ion implantation or the use of a material with moderate resistivity can prevent polarization and charge build-up (64–68). In general, modest surface quality and poor metal adherence, added to high manufacturing costs, have resulted in moderate success and limited application.

Optimization of Design and Operation

A particular effort has been undertaken to optimize the design of the detectors for high-rate tracking of minimum ionizing particles. With a required operating gain of a few thousand, a reachable gain up to 10^4 is considered necessary to ensure safe operation. Although thin anodes provide the best performance, practical considerations restrict the widths to between 5 and 10 μm. Decreasing the gap between

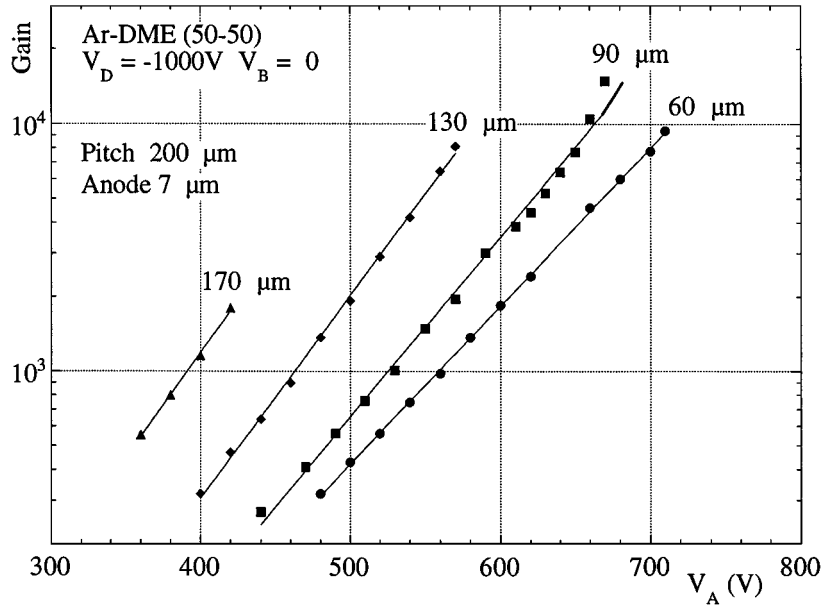

Figure 11 Gain versus anode voltage measured with cathode strip widths ranging from 170 μm to 60 μm and a fixed pitch of 200 μm. V_D and V_B are the drift and back-plane potentials.

strips by making the cathodes wider helps to reduce the voltage required for a given gain. However, for very narrow gaps, presumably because of imperfections in the lithography and substrate, discharges limit the maximum gain (Figure 11) (69). The optimum choice is a width around 90 μm, an aspect ratio (metal to insulator) of $\sim$50%. A detailed study of the single-electron noise spectra close to the maximum confirms the hypothesis that discharges can be triggered by avalanches initiated by electrons released at the cathode edge, by ion bombardment and field effect (69).

Detection of fast particles in a few millimeters of gas requires the use of gases with favorable ionization statistics. The best results have been obtained using dimethyl-ether (DME). At a pressure of 1 bar, minimum ionizing particles have 55 ionizing collisions per centimeter in DME, compared with 25 in argon and 15 in neon. To reduce the operating voltage, DME is mixed with noble gases (70–73). Figure 12 shows gain versus voltage for a variety of mixtures containing DME. Other gases tested include mixtures with CF_4 (74), which have the advantage of a faster drift velocity and reportedly prevent or even reverse aging processes in multiwire chambers.

Assembly of Detector Modules

Several schemes have been used to assemble MSGC detectors. For laboratory measurements, a vessel with high voltage and signal feed-through is convenient

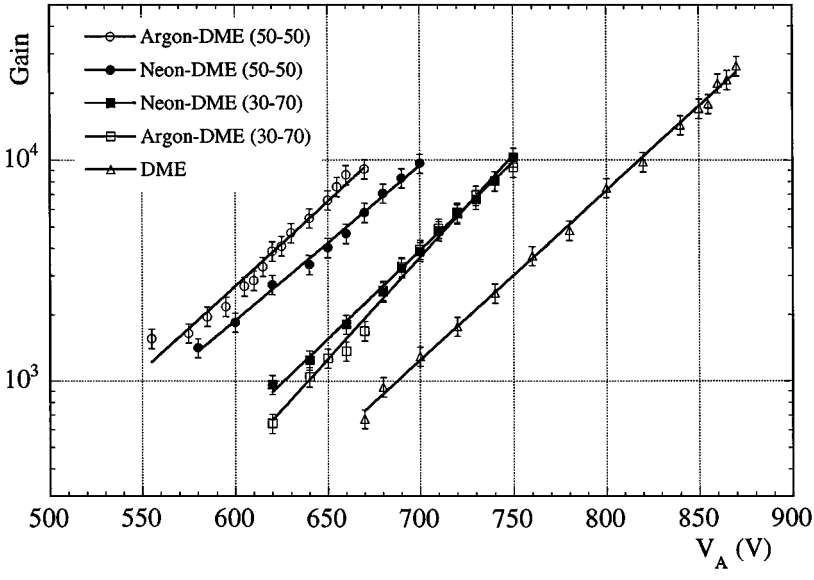

Figure 12 Examples of absolute gain measured, as a function of anode voltage, in several mixtures of noble gases and dimethyl-ether.

for testing individual plates. Some experiments have adopted a similar scheme, with several arrays of plates mounted in a large gas box (75). Lighter and cheaper assemblies have been developed for large modular arrays. As shown schematically in Figure 13, a module is manufactured with a thin, rectangular insulating frame glued directly on the rigid engraved substrate; a second thin glass plate, conductive on the inner side, is glued to the frame and constitutes the drift electrode (76). Holes in the frame provide gas inlet and outlet.

Microstrip plates with nonparallel strip geometry serve the specific needs of forward trackers in particle physics. In the so-called keystone or wedge-shaped geometry, strips fan out from a minimum to match the angular divergence of tracks. Proper width and spacing of the strips can provide a uniform gain despite the varying pitch (77, 78). Several plates can be assembled edge to edge inside a common box, with the readout electronics inside or outside the gas volume. Figure 14 shows a prototype with eight wedge-shaped MSGC plates mounted in contact in a semicircular module (the so-called closed banana) (79), developed for the CMS Forward MSGC detector. The geometry of the joints (or cracks) has been thoroughly studied to minimize detection losses (80, 81).

In most MSGC designs, anode and cathode strips are, for convenience, connected on opposite sides. The electric field is strongly perturbed in the vicinity of the ends of the strips; the cathode-end side is particularly affected, and discharges can easily occur even at low voltages. Several studies have attempted to optimize the geometry of the strip ends, with rounded tips and/or an increase of the gap, in

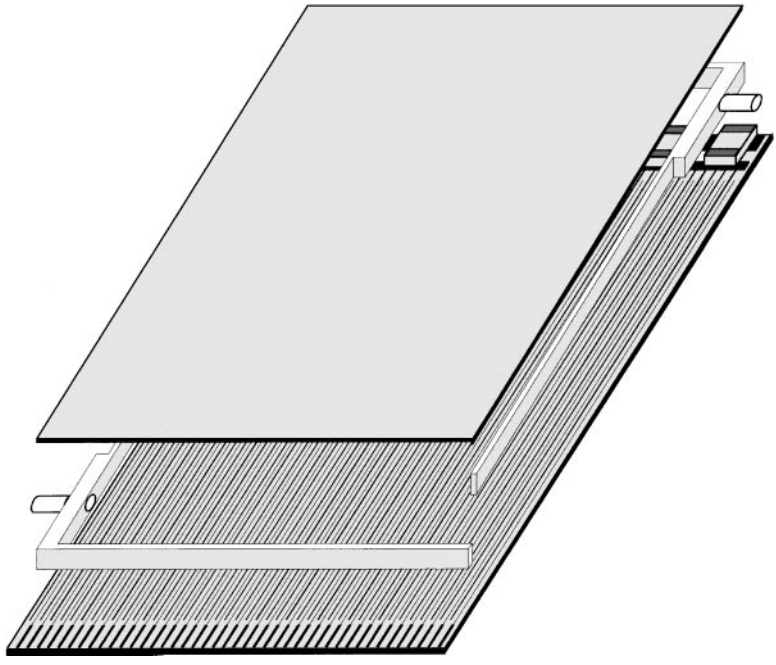

Figure 13 Schematics of the light mechanical assembly of a microstrip gas chamber module. Typical dimensions of the substrate engraved with the metal strips are 10×10 cm^2; thin insulating frames are glued on the plate, and a metal-coated top is pasted as a drift electrode. The gas inlets are provided through holes in the frame.

order to reduce the field singularities (82, 83). In order to reach the high voltage required for detection of small amounts of ionization, coating (passivating) the critical area with an insulator is an effective method to avoid these edge effects. The coating material must have excellent dielectric rigidity and low outgassing, and the curing method must be compatible with the other components.

Detection and Localization of Charged Particles

Prototypes of various designs have been extensively tested in the laboratory and in test beams to study the detection of minimum ionizing particles (78, 84–94). Small but complete systems have also been successfully used as high-precision tracking systems in physics experiments (75, 95–99). Several highly integrated readout circuits that were originally developed for the requirements of silicon microstrips have been adapted to MSGCs. They generally have fast shaping times, typically 30 to 60 ns (100). Because of the particular characteristics of signals induced by the slow motion of ions, there is a considerable reduction of the detected charge (the so-called ballistic deficit). The signal shapes under various load conditions, and their effects on resolution, have been analyzed in detail (101, 102). Some

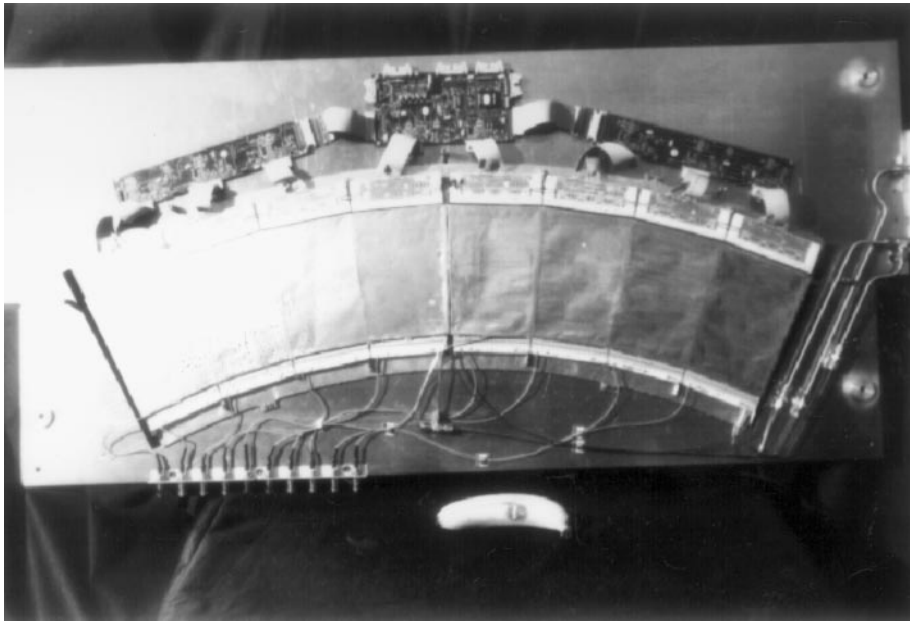

Figure 14 An eight-plate module, complete with readout electronics, developed for the forward detector of the Compact Moon Solenoid (CMS) experiment. Each microstrip plate measures about 10×16 cm^2.

calculations include a detailed Monte Carlo simulation of the ionization statistics and charge collection processes (103).

At high rates, the electron collection time must be minimized so as to reduce the strip occupancy and thus the probability for signal overlap. This can be achieved by narrowing the detection gaps (2–3 mm), selecting a fast gas mixture and high values of the drift field. Figure 15 gives an example of the distribution of the total charge collected for minimum ionizing tracks of perpendicular incidence on an MSGC operating at gains of a few thousand; the distribution has the characteristic Landau shape. The small peak at the left represents the noise. The signal-over-noise ratio, defined as the most probable value of the charge divided by the standard deviation of the noise, is only around 15. At higher voltage, more favorable values are attainable but operation can become unsafe. Figure 16 shows examples of efficiency plateaus for relativistic particles, perpendicular to the detector, and for different gases (87).

Position accuracy of better than 40 μm rms was demonstrated in early works (104) for perpendicular tracks and has been confirmed by many measurements. The cluster size, or mean number of anode strips with signals over threshold for each track, is around 1.5 strips for 200 μm pitch. Under these conditions, two tracks that are 500 μm apart can be fully resolved (78). Because of the dispersions

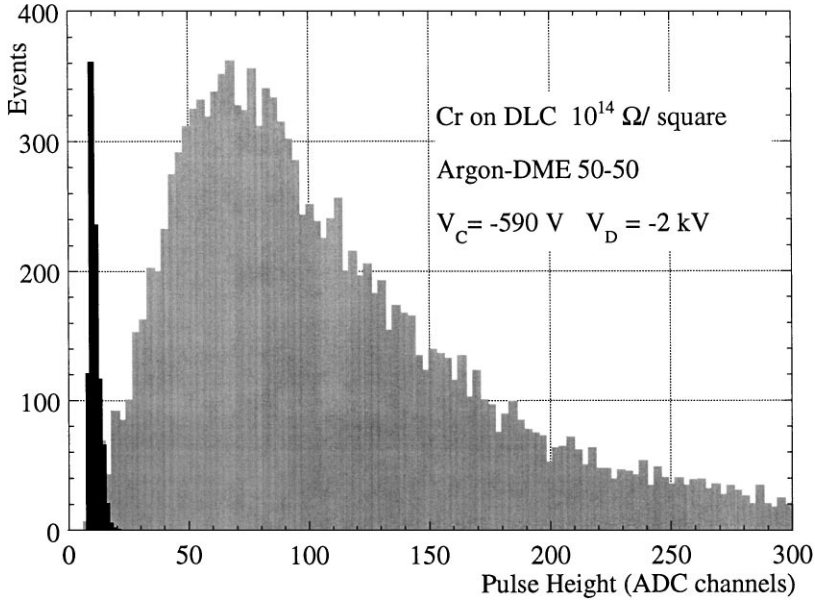

Figure 15 Total charge spectrum recorded on the anodes for minimum ionizing tracks in a 3-mm-thick microstrip gas chamber, made with chromium strips on a diamond-like coated substrate. V_C and V_D are the cathode and drift voltages, the anodes being grounded.

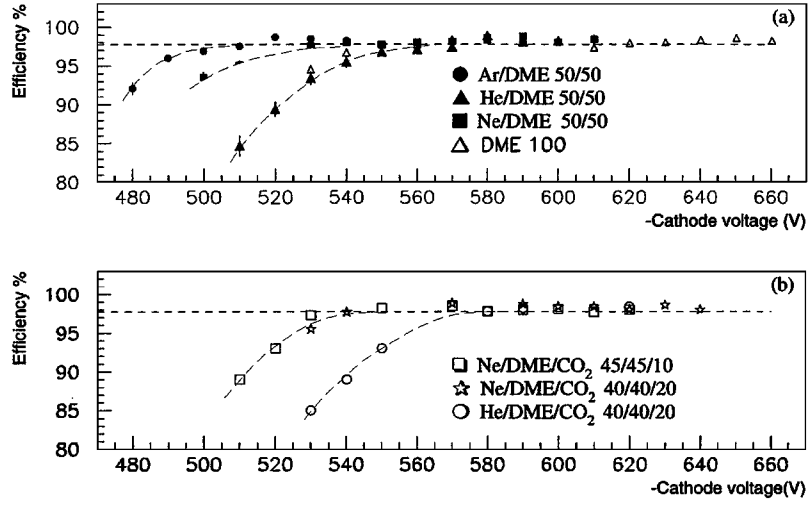

Figure 16 Detection efficiency of microstrip gas chambers for minimum ionizing particles, as a function of cathode voltage, in several gas mixtures.

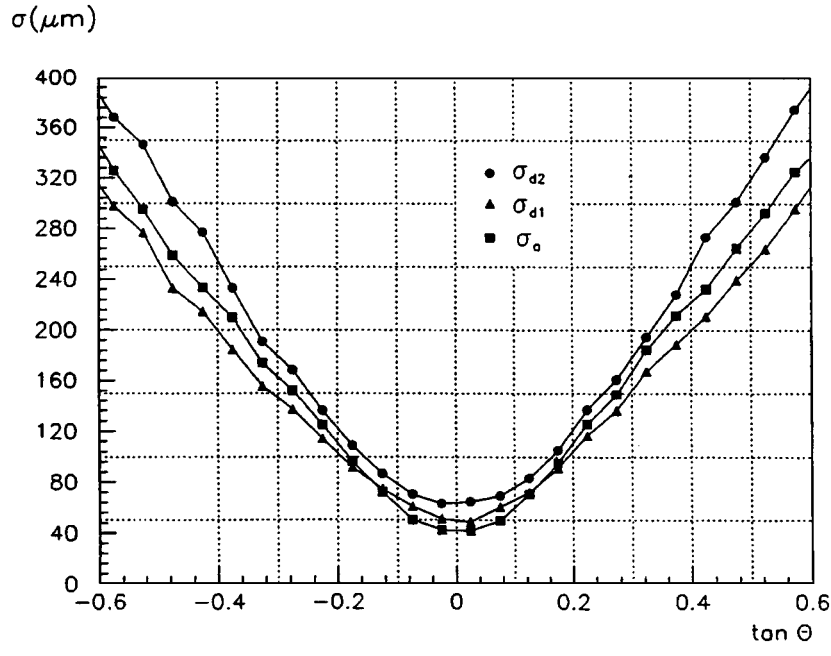

Figure 17 Standard deviation of the position resolution (rms) as a function of angle of incidence. The origin corresponds to tracks perpendicular to the plate. The three curves correspond to different reconstruction algorithms.

introduced by the primary ionization statistics, the accuracy worsens for tracks at increasing angles to the normal relative to the gap, as shown in Figure 17 (105). The cluster size widens correspondingly, and because of the sharing of charge between strips, it becomes increasingly difficult to obtain good detection efficiency.

Operation in strong magnetic fields is necessary in some experiments. A nonzero magnetic field component in the direction of the drift results in a deflection of the electrons, the Lorentz angle. Its value depends on gas and electric field and affects the drift velocity. This deflection can degrade the resolution and efficiency. DME-rich mixtures and high drift fields tend to diminish the deflections; at 4 Tesla, the Lorentz angle can be reduced to around 15° and can be compensated, at least for a parallel-tracks field, by a slight rotation of the detectors. This solution has been adopted for the CMS tracker, based on systematic measurements with prototype MSGCs operating in strong magnetic fields (106, 107).

Two-Dimensional Readout

The fast collection of electrons and the retrograde motion of ions induce signals on the anodes and all surrounding electrodes. The back-plane electrode can be segmented to provide an independent coordinate. The size of induced signal depends

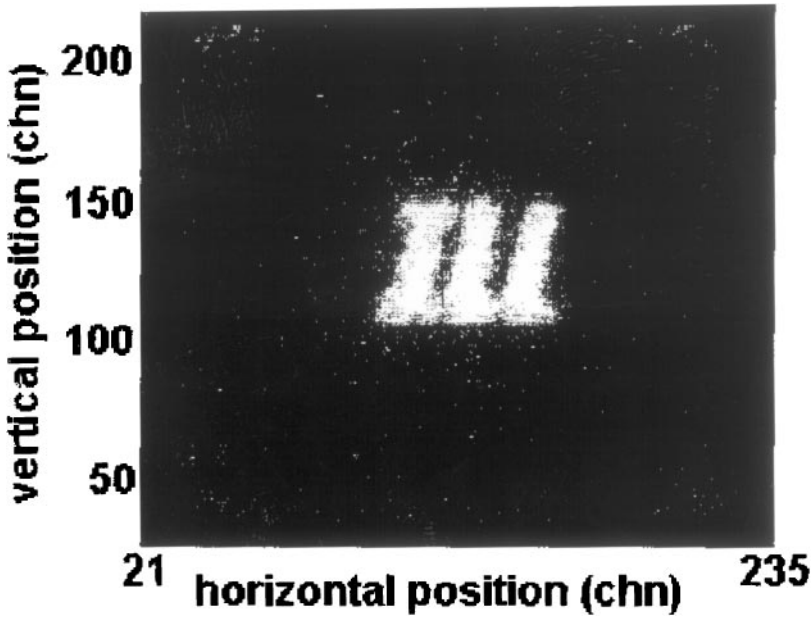

Figure 18 Example of two-dimensional imaging capability. The microstrip chamber with back-plane readout was exposed to a thermal neutron flux through a mask.

on the ratio between pitch and substrate thickness (108). When a higher negative potential is applied to the back-plane, the signal increases—at the expense of a reduced rate capability (109). Figure 18 shows a neutron-absorption image obtained with an MSGC with a two-dimensional readout.

One way to increase the back-plane signal is to leave the cathodes floating (110). Removing the metal from most of the strip surface, leaving only the edges to define the field, permits larger signals on the back-plane (108); however, to avoid severe charge build-up problems, substrates with reduced resistivity are necessary. MSGCs built on electron-conducting glass substrate have shown reasonably stable behavior, at least for moderate rates. In the so-called asymmetric or virtual cathode chamber (108, 111), cathodes are removed altogether, and performance is stable.

Using integrated-circuits technologies, a double metal structure, separated by a very thin insulating layer, can be grown on the top of a thicker substrate. Two-dimensional devices of this design have been built, with either a few microns thick ion implanted silicon oxide (112, 113) or a thicker polyimide film separating the two metallic coatings (114–116). With almost identical signal amplitudes on the anodes and back-plane strips, excellent correlation between the two coordinates has been demonstrated. This design requires that the thin insulator hold the operating voltage between cathodes and back-plane without leakage or discharge. This turns out to be rather difficult with thin silicon oxide films; polyimide, which can be grown up to several tens of microns, is a better choice. Because of its intrinsic high

cost and size limitations, this semiconductor technology has not yet been exploited for large systems.

Long-Term Performance: Discharges and Aging

Despite their promising performance, experience with MSGCs has raised doubts about long-term behavior. Two major problems, their relevance depending on the application, have arisen: rare but often damaging discharges, and slow but continuous deterioration (aging) during sustained irradiation.

Discharges during operation are a permanent problem with all gas micropattern detectors. They have been extensively analyzed in studies ranging well beyond the MSGC work (70, 117–122). Whenever the total charge in the avalanche exceeds a value between 10^7 and 10^8 electron-ion pairs (Raether's limit), an enhancement of the electric field in front of and behind the primary avalanche induces the fast growth of a long, filament-like streamer. In the high fields and narrow gaps typical of micropattern devices, this leads to discharge, with damaging effects on the strips (Figure 19). Depending on conditions, a discharge can damage the strip or, in the worst case, produce a local short or open circuit. Metals with low melting points, such as gold and aluminum, are easily damaged, whereas others such as chromium and tungsten are more resistant (123, 124). At the gains required for the detection

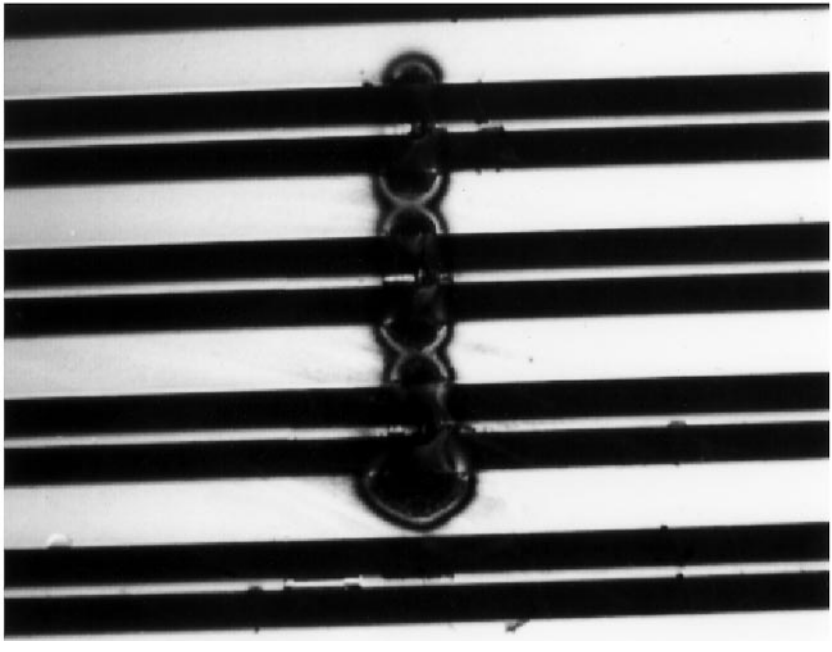

Figure 19 Close view of the strips on a plate in the region of a discharge. Note extensive damage to the strips.

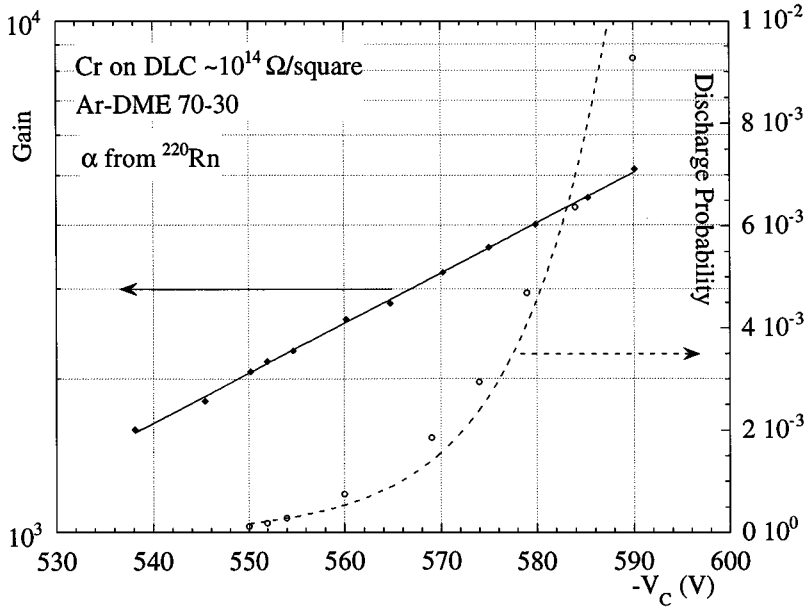

Figure 20 Gain curve, measured at low irradiation rate, and discharge probability under exposure to an internal alpha-particles emitter, as a function of cathode voltage.

of minimum ionizing particles in thin gaps, typically above 2000, the accidental release of larger amounts of ionization easily brings the total charge above the limit. For reasons that are not completely understood, a high rate of low ionizing radiation produces a similar effect.

The behavior of detectors exposed to large ionization losses can be emulated in the laboratory by exposure to alpha particles, from an external source or internally emitted by ^{220}Rn injected in the gas flow and generated by a cartridge containing thorium oxide. A very fast increase of the discharge with the operating voltage is observed at gains above a few thousand, as shown in Figure 20 (125). Detailed studies of the process, extended to other designs of detectors, suggest that all single-stage micropattern detectors suffer from the same basic limitation, which can be overcome if the multiplication process is shared between cascaded devices (120).

Various schemes have tried to limit the damage caused by discharge. It is helpful to reduce the available energy by connecting small groups of strips to the voltage with limiting resistors, but this correspondingly increases the opposite-polarity signal pickup. Alternatively, adding a series resistor, $\sim$1 kΩ, at the amplifier's input limits the energy flow but affects the signal rise time (96). Coating the cathode edges with a thin polyimide insulator, or so-called advanced passivation, has been claimed to prevent discharges up to very high gains (126), but this observation is not confirmed by other authors (119, 120).

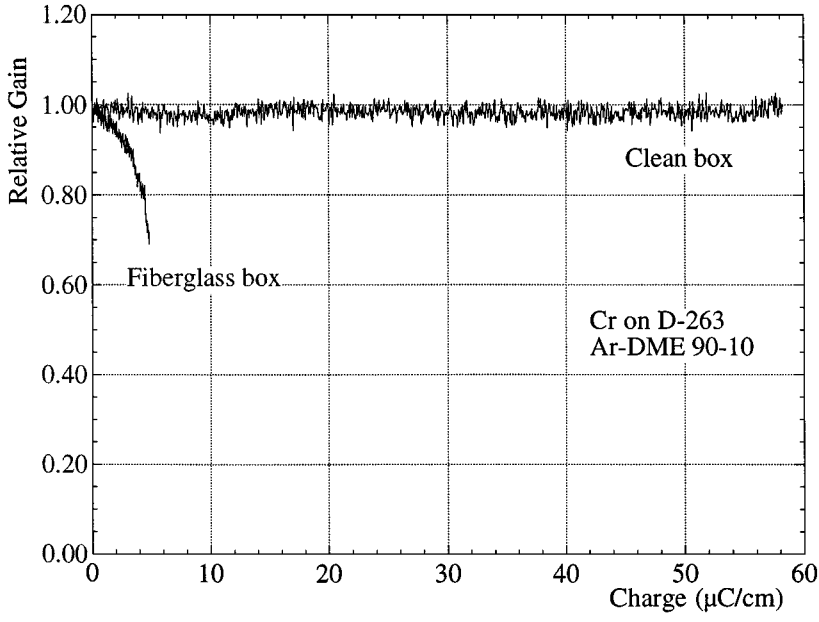

Figure 21 Comparison of aging rate under irradiation for identical plates, mounted either in a conventional fiberglass assembly or in a clean container.

Aging, the slow degradation of performance during sustained irradiation, is a problem encountered with most gaseous counters and has been extensively studied experimentally (for a review see 127, 128). The observed permanent damage to the plates has been imputed to the production of polymeric compounds in the avalanches, which stick to the electrodes or to the insulator, perturbing the signal detection and inducing discharges. MSGCs are particularly prone to aging, possibly because of the small effective area used for charge multiplication. Organic gases, such as hydrocarbons, induce very fast aging, whereas others, such as dimethyl-ether and carbon tetrafluoride, allow more extended lifetimes. A careful selection of the operating gas and of the materials used in manufacturing is mandatory to assure survival of the devices in a high-radiation environment (129, 130). Figure 21 illustrates the dramatic difference in aging rate between identical plates, one using a conventional detector assembly with fiberglass and epoxy and the other using a clean containment vessel (131). All other conditions being equal, use of low-resistivity substrates permits higher levels of exposure without loss of gain (40, 49, 132), possibly by reducing the effect of thin deposits on the field. The choice of metal for the strips also appears to play an important role (71), gold being the best (Figure 22) (133).

Under optimal laboratory conditions, many groups have demonstrated long-term survival of MSGCs without degradation up to a collected charge above 100 mC cm^{-1} (33, 35, 40, 67, 71). Figure 23 shows a measurement that used

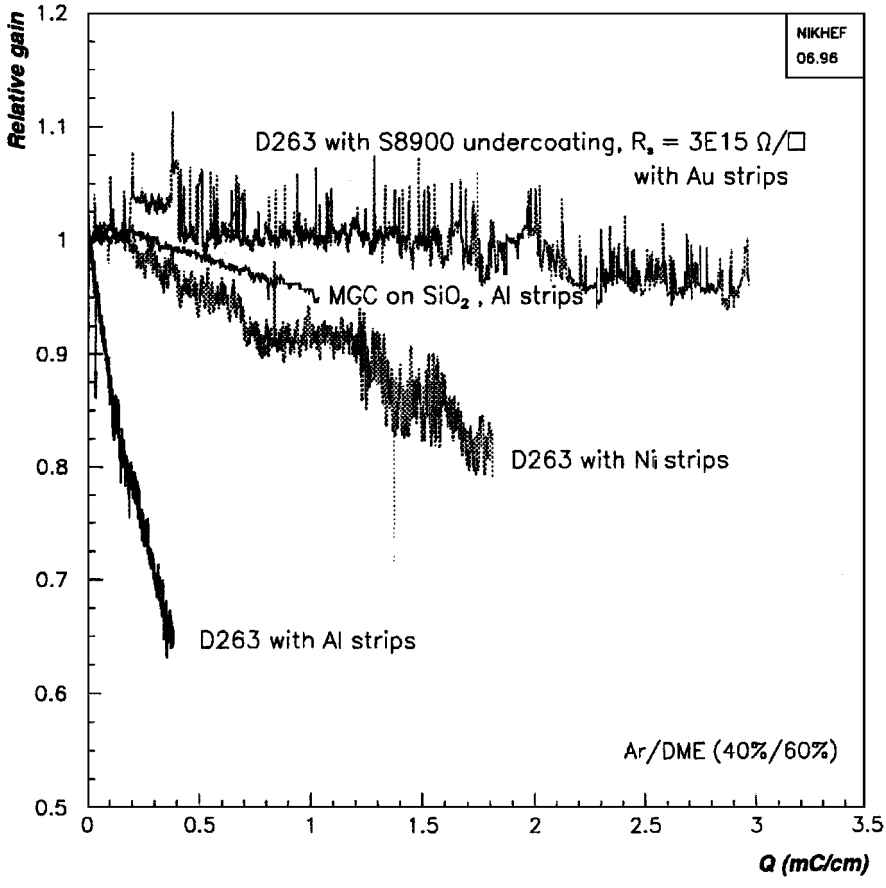

Figure 22 Gain drop, or aging, under sustained irradiation of microstrip plates manufactured on insulating and semiconducting substrates, for different strip metals.

a plate made with chromium strips on low-resistivity glass. Similar results have been obtained using MSGCs manufactured on thin electron-conducting layers (26, 33, 63).

Other Developments and Applications

Though originally conceived to detect neutrons and X-rays, MSGCs owe most of their development to the demanding requirements of high-rate tracking of charged particles. Many other applications have been developed, often with large improvements in performance.

Following the successful initial development, the group at ILL built and operated several position-sensitive neutron detectors. The largest system, the D-20 spectrometer, includes 50 medium-sized MSGC plates operated in a ^{3}He-CF_4 gas

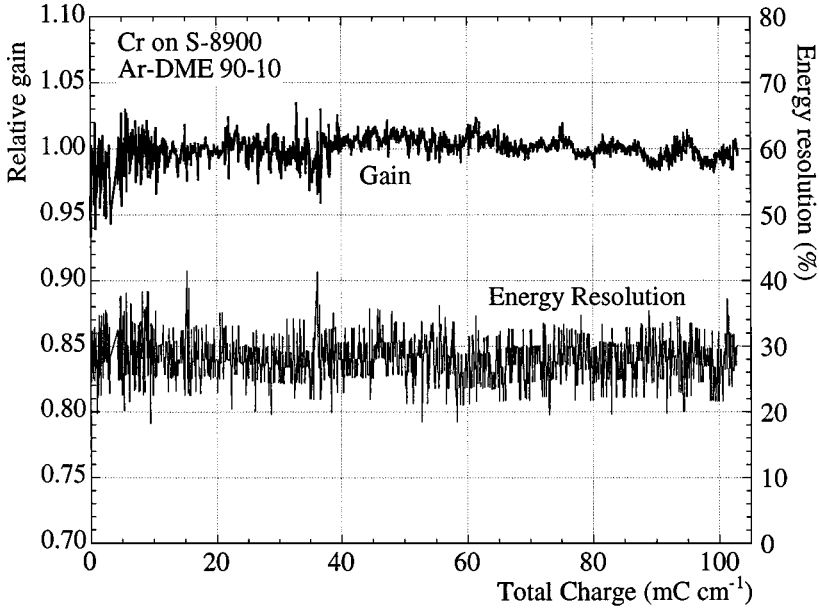

Figure 23 Gain and energy resolution as a function of irradiation measured with a microstrip plate made on electron-conducting glass. No deterioration is observed up to a total collected charge of 100 mC cm^{-1}.

mixture for optimal efficiency and performance. A similar, smaller system has been used to study single-crystal neutron diffraction (134).

Astrophysics has exploited the excellent energy and position resolution of these devices for the detection of soft and intermediate-energy X-rays (135). The high rate capability, particularly if coupled to digital readout electronics, permits the faster recording of absorption radiographs (136). The high rate capability is also exploited in detectors for synchrotron radiation facilities (137). With gadolinium converter foils as drift electrodes, MSGC plates have been used for the imaging of thermal neutrons (138, 139).

The operation of MSGCs at low pressures has been extensively studied; a two-stage gain process, an initial parallel plate multiplication gap followed by the normal MSGC, permits the large gains needed for single-electron detection (140). With the addition of an internal photosensitive electrode, such as evaporated cesium iodide, the device becomes a detector for ultraviolet light (141) with good position resolution. Secondary emission from low-density layers of cesium iodide or diamond-like carbon has been used to detect charged particles in devices capable of sub-nanosecond timing and with angle-independent position measurement (142).

MSGCs with back-plane padded readout schemes have been considered for the construction of improved time-projection chambers, capable of better multitrack

resolution than the classic design. Other advantages of such schemes are the possibility of using short and nonparallel anodes, higher rate capability, and reduction of ion feedback (143, 144).

High-pressure operation has been investigated to allow the use of MSGCs as detectors for hard X-rays in medical diagnostics. Despite the need for increasingly high operating voltages, gains sufficient for detection could be reached in xenon gas mixtures (39, 145).

Various authors have studied the scintillation properties of MSGCs (146–148). Electron multiplication has been demonstrated using an MSGC in liquid xenon, a potentially far-reaching development (149).

ALTERNATIVE MICRO-ANODE STRUCTURES

Microgap and Small-Gap Chambers

As discussed above, one way to obtain two-dimensional projective readout in MSGCs is to reduce the thickness of the insulator separating the anodes from the back-plane. This can be achieved with microelectronics technologies, specifically the deposition of a few microns thick insulating film between metallic layers. The possibility of patterning electrodes and the insulating layer has led to the development of the microgap chamber (MGC) (150, 151), a structure in which the back-plane acts as a cathode, with thin anodes on insulating strips (see Figure 24). The very small gap between anodes and cathodes allows a very high electric field, resulting in faster signal rise time and shorter ion collection—a distinctive advantage of such devices. Two-dimensional readout is obtained by patterning the cathode plane with perpendicular strips or pads interconnected in a ladder-like structure for small-angle stereo readout.

Large gains, above 10^4, have been obtained with a MGC. Mixtures of neon and dimethyl-ether seem to be particularly advantageous. Fast response, good localization accuracy, and high rate capability have been demonstrated (152, 153).

A high dielectric rigidity of the insulator between anode strips and cathodes is the key to stable operation. Early devices employed a silicon oxide insulating layer a few microns thick, which was applied by chemical vapor deposition. Experience has shown, however, the non-negligible probability of local defects (punch-through), making it very difficult to fabricate larger-area detectors (154). In later MGC models, a thicker polyimide coating (several tens of microns thick) has been applied to ensure better rigidity (155, 156). Thin polyimide strips have also been used to passivate the potentially dangerous high-field regions at the separations between cathode strips.

Several authors have studied operating properties of MGCs manufactured with different metals and a range of geometrical parameters (50, 124, 157), as well as the resistance of the devices to local discharges (123). For potential medical applications, MGC operation in xenon and krypton at pressures up to six bars has also been investigated (158, 159).

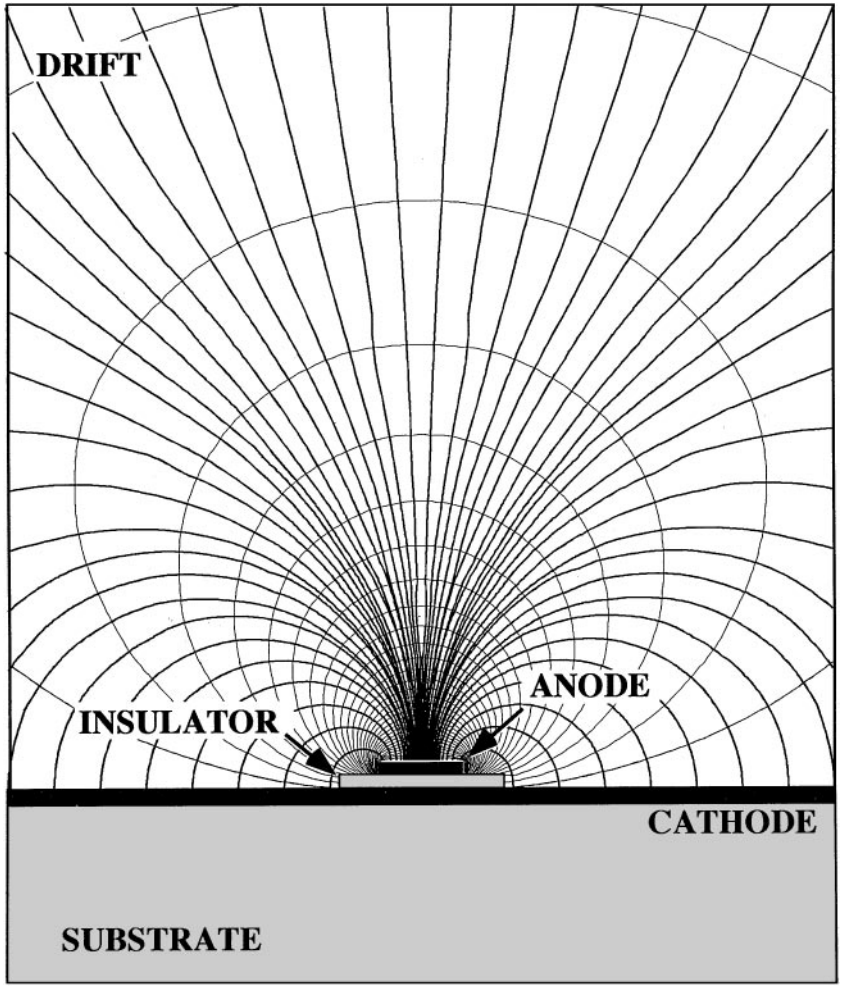

Figure 24 Equipotential and electric field lines for the microgap chamber.

Several variants of the basic microgap structures have been tested to improve their performance and reliability, with particular attention to the onset of discharges (156). Figure 25 shows two recently developed structures called small-gap chambers, which have been successfully tested in the laboratory and in beam conditions (160, 161).

Microdot Chamber

Manufactured with metal-oxide semiconductor technology, the microdot chamber (15, 154, 162) consists of a dense pattern of individual proportional counters made up of anode dots surrounded by annular cathodes. Field-defining rings can be

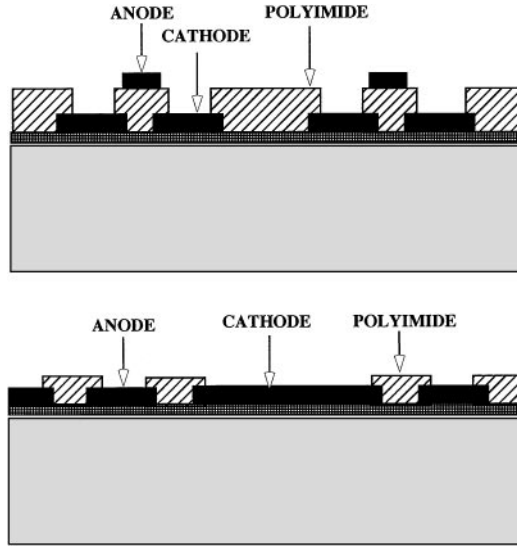

Figure 25 Two variants of small-gap chambers, using thick polyimide ridges to prevent the onset of discharges.

added to improve the operation, as shown in Figure 26. The structure is built atop a thin oxide layer grown on a silicon substrate. To avoid charge build-up, the oxide can be ion implanted or the device can be coated with a semiconducting layer of boron-doped amorphous silicon carbide (163). For convenience of readout, the dots can be interconnected by a metal layer buried under the oxide. The role of the guard rings is to reduce field distortions induced in the multiplying cell by the interconnections. They also help prevent the onset of discharges. Small microdot devices have been tested in a variety of conditions and gas fillings; Figure 27

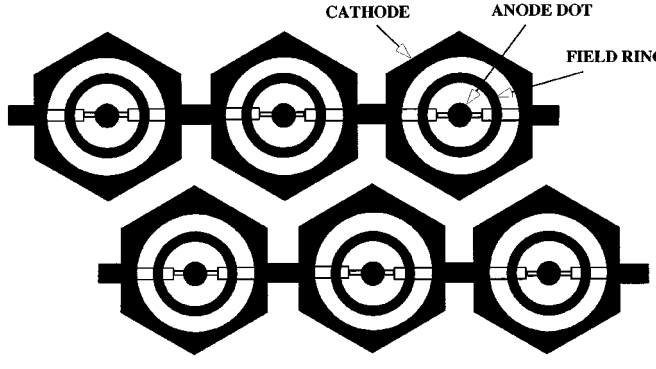

Figure 26 Schematics of the microdot chamber. A pattern of metallic anode dots surrounded by field and cathode electrodes is implemented on an insulating substrate, using microelectronics technology. Anodes are interconnected for readout.

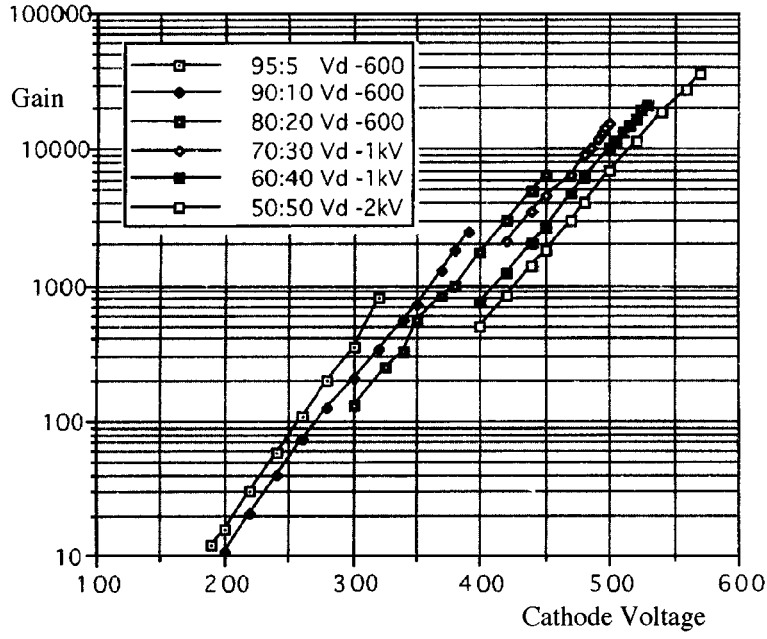

Figure 27 Examples of the very high gains attained with the microdot detector in various argon–dimethyl ether mixtures.

gives an example of the large gains that can be attained in argon-DME mixtures. Thanks to its fast response and its use of the pixel structure, the microdot is ideal for applications requiring the simultaneous detection of multiple hits, such as Cerenkov ring imaging. Attempts to detect single photoelectrons, however, have been only partly successful, despite the large gains, because of the high level of noise induced by the large capacitance of the cells (164). This disadvantage can be overcome by operating the detector at low pressures, where gains in excess of 10^7 can be reached by exploiting parallel-plate preamplification (165). The microdot detector is the only device that could withstand high gains under alpha-particle irradiation in a recent systematic study of discharge properties in micropattern detectors (120).

NOVEL MICROPATTERN DETECTORS

Thin-Gap Parallel-Plate Structures, Micromegas

The successful development of multiwire and microstrip structures has somewhat sidestepped the research on gas detectors that exploit the multiplication in uniform fields. Parallel-plate multipliers not only are mechanically sturdier but also have better energy resolution and higher rate capability. However, experimental data and

theoretical considerations indicate that the maximum proportional gain in parallel-plate chambers is limited by the total amount of charge in the avalanche, around 10^7–10^8. Above this value, called the Raether limit, transition to a streamer occurs, followed by breakdown. This has been confirmed under a wide range of operating conditions and multiplying gaps (166–168). The exponential dependence of gain on the gap has also discouraged the construction of large-area devices.

It has been recently suggested that in submillimeter gaps exceptionally large gains could be attained, reaching the upper limit allowed by the Raether condition (14, 122). This has led to the introduction of the micromesh gaseous chamber (micromegas) (14), shown in Figure 28. The detector consists of a thin metal grid stretched at a very small distance, 50–100 μm, above a readout electrode. With a very high field applied across the gap, typically above 30 kV/cm, electrons released in the upper drift region are collected and multiplied. The mesh itself, a standard component in high-resolution TV screens and usually made of

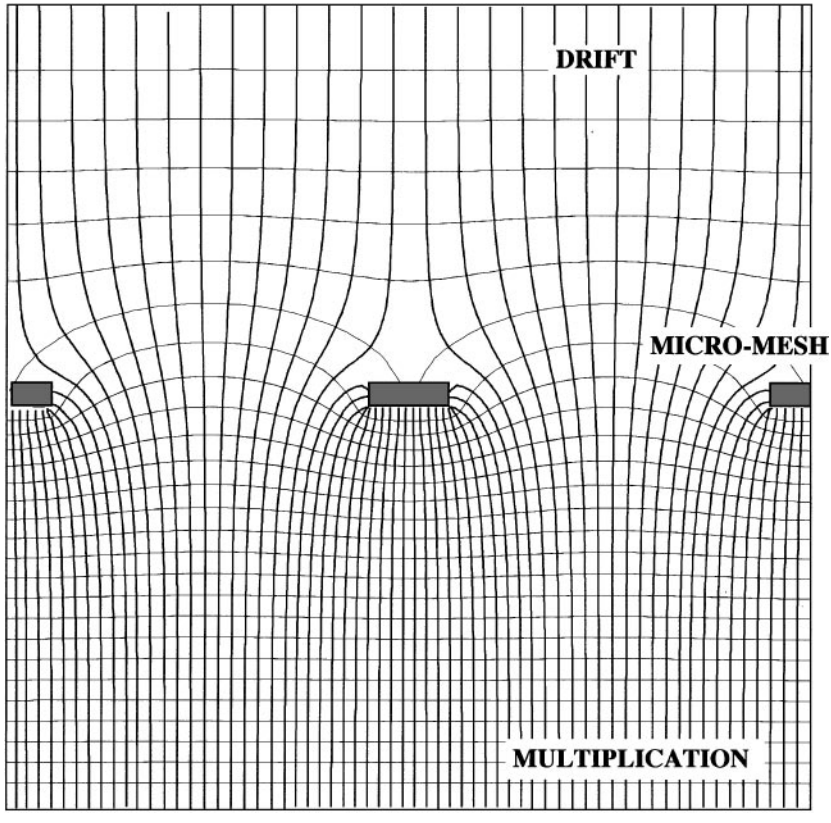

Figure 28 Schematics and electric field map in the micromegas. A metallic micromesh separates a low-field, or drift, region from the high-field multiplication region.

nickel, is commercially available in various sizes and shapes. Regularly spaced supports (insulating fibers or pillars) guarantee the uniformity of the gap, at the expense of a small, localized loss of efficiency. Essentially an avalanche counter with a Frisch grid, the micromegas exploits the saturating characteristics of the Townsend coefficient at very high field to reduce the dependence of gain on the gap variations, thus improving the uniformity and stability of response over a large area. The micromegas retains the rate capability and energy resolution of the parallel-plate counter. Thanks to the small gap and high field, positive ions move very quickly, and most are collected by the cathode mesh; this prevents space-charge accumulation and induces very fast signals with only a small ion tail, 50–100 ns wide. The micromegas can operate at very high particle fluxes; Figure 29 shows a measurement of current as a function of voltage, measured at increasing rates of 20-MeV incident protons. The curves are parallel in a wide range of ionization

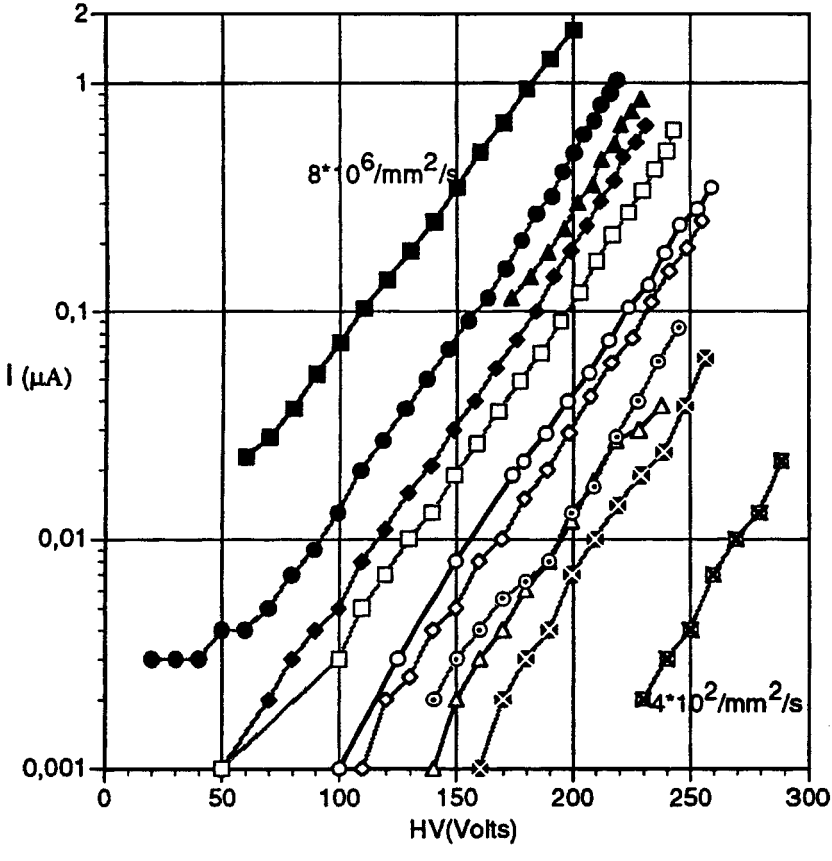

Figure 29 Detected current with the micromegas, measured at increasing flux of ionizing particles.

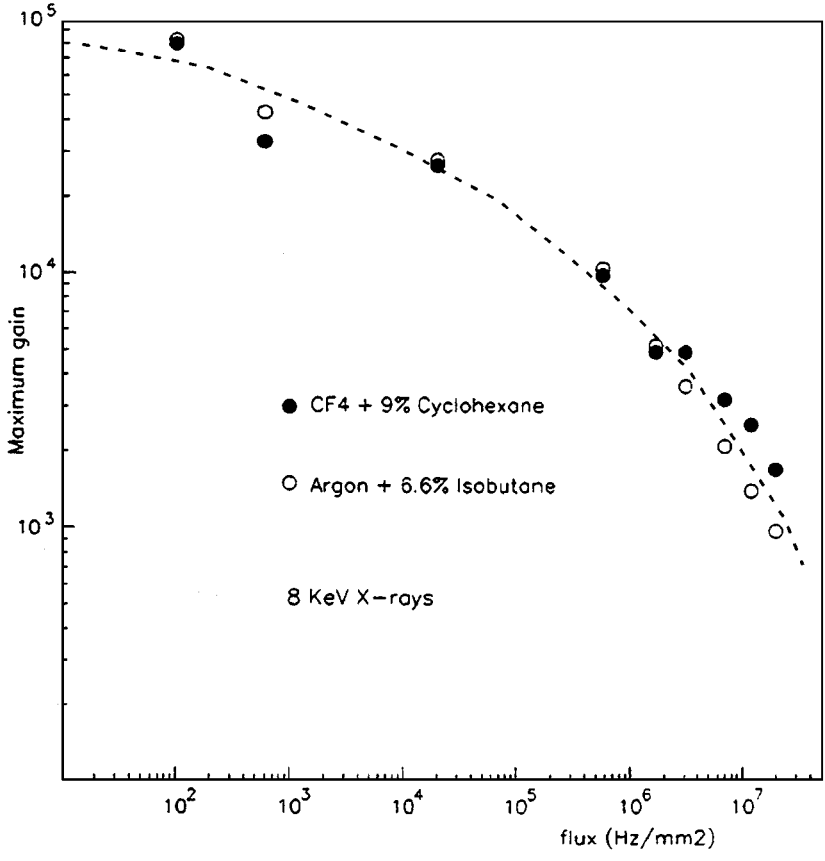

Figure 30 Maximum gain in the micromegas as a function of the incident 8-keV X-ray flux, in two gas mixtures.

densities, demonstrating the absence of space-charge distortions. The maximum gain, however, depends on the amount of charge, as seen in Figure 30, which shows the maximum gain attained with the detector as a function of the X-ray flux (169).

Efficiency and localization properties of the detector have been studied with several exposures to particle beams (170). Reasonable efficiency plateaus have been obtained for minimum ionizing particles traversing perpendicular to the chamber. Probably because of the poorly quenched gas mixtures used for the tests, which permit operation at moderate voltages, the lateral extension of the avalanche, or cluster size, was rather large (around 1 mm). Further studies using better quenched gas mixtures and fast readout electronics have substantially reduced cluster size, at the expense of a somewhat reduced length of the efficiency plateau (171).

Recent studies have demonstrated that the micromegas, like all single-step micropattern detectors, suffers from the basic limitation in gain (a few thousand) when exposed to heavily ionizing tracks (120).

Trenches and Holes, CAT and Micro-CAT

The gain of a parallel-plate counter depends exponentially on the gap thickness, making it difficult to obtain a uniform response over large areas. The problem is exacerbated by the strong attraction between electrodes. Several solutions have been proposed involving the insertion of an insulating interface between the electrodes. An early example is the microtrench gas counter, consisting of a sequence of wide anode strips buried in insulating channels with cathodes on the top (172). Charge amplification within narrow holes in a composite metal-insulator stack has also been observed with the high-density drift chamber, a device designed for the conversion and detection of hard X-rays (173).

In the compteur à trous (CAT), holes drilled through a metal-insulator sandwich concentrate the field lines converging from a drift volume into a region of high field, where charge multiplication occurs (see Figure 31) (13). Even with relatively large holes, the collection and focusing properties of the field result in good energy resolution at proportional gains up to 10^4 (Figure 32). The detected signal has, as expected, a fast electron and a slower ion component; the time length of the ion tail depends on the gap (several microseconds for one millimeter) and can be reduced to a few hundred nanoseconds for narrower gaps. Several variations of the structure have been studied, with multiple holes and different shapes of the insulator plate designed to minimize charge build-up processes.

Micro-CATs are structurally similar to micromegases, but like CATs, they use cathodes with round holes. They were developed for the realization of two-dimensional X-ray imaging detectors (174). The effect of the hole geometry and gap thickness on gain and energy resolution has been studied for a variety of gases and operating pressures, up to 6 bars. To aid medical applications, the authors developed a cellular resistive readout using a resistive anode foil that is padded with conducting lines and forms a regular matrix of nodes, each connected to a charge-sensitive amplifier. With a detector operated at 3 bars, a position accuracy of 200 μm (fwhm) for 8-keV X-rays has been demonstrated (175).

The Gas Electron Multiplier

To obtain larger gains with parallel-plate structures, Charpak & Sauli (176) devised the multistep avalanche chamber. Made with a succession of metal meshes, the detector multiplied ionization electrons injected from a drift region into a high field. A fraction of the avalanche was then transferred through a lower field region into a second element of multiplication, a parallel plate or a wire chamber. Despite the loss of charge in the transfer from high to moderate fields, effective preamplification factors of several hundred were possible. Followed by a standard MWPC, the device permitted the high gains necessary to detect single photoelectrons (177).

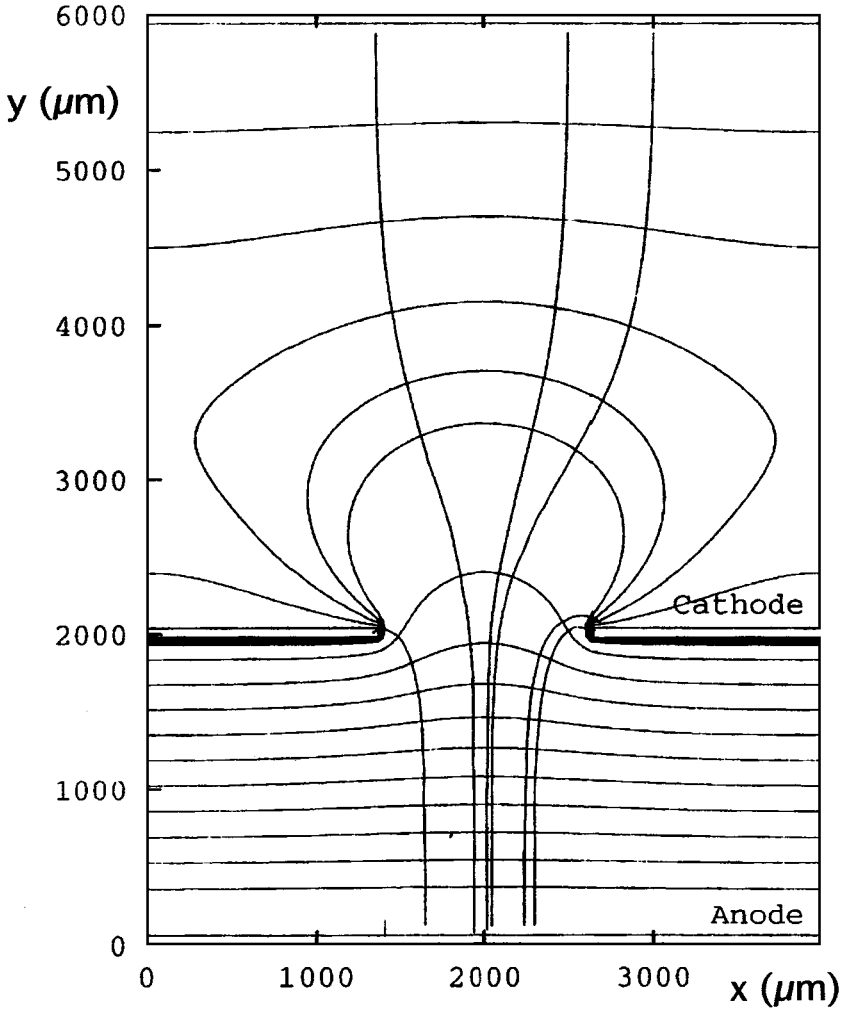

Figure 31 Schematics and fields in the compteur à trous.

The multistep chamber was mechanically complex to implement and had only limited success, but demonstrated the great potential of subdividing the gain among several cascaded elements separated by low-field gaps.

The gas electron multiplier (GEM), introduced by Sauli in 1996 (16), consists of a thin, metal-clad polymer foil chemically perforated by a high density of holes, typically 100/mm^2 (Figure 33, color insert). As shown in Figure 34, with a suitable choice of voltages, all electrons released by ionization in the overlying gas layer are sucked into the holes, where charge multiplication occurs in the high electric field. Most of the electrons generated in the avalanches transfer into the

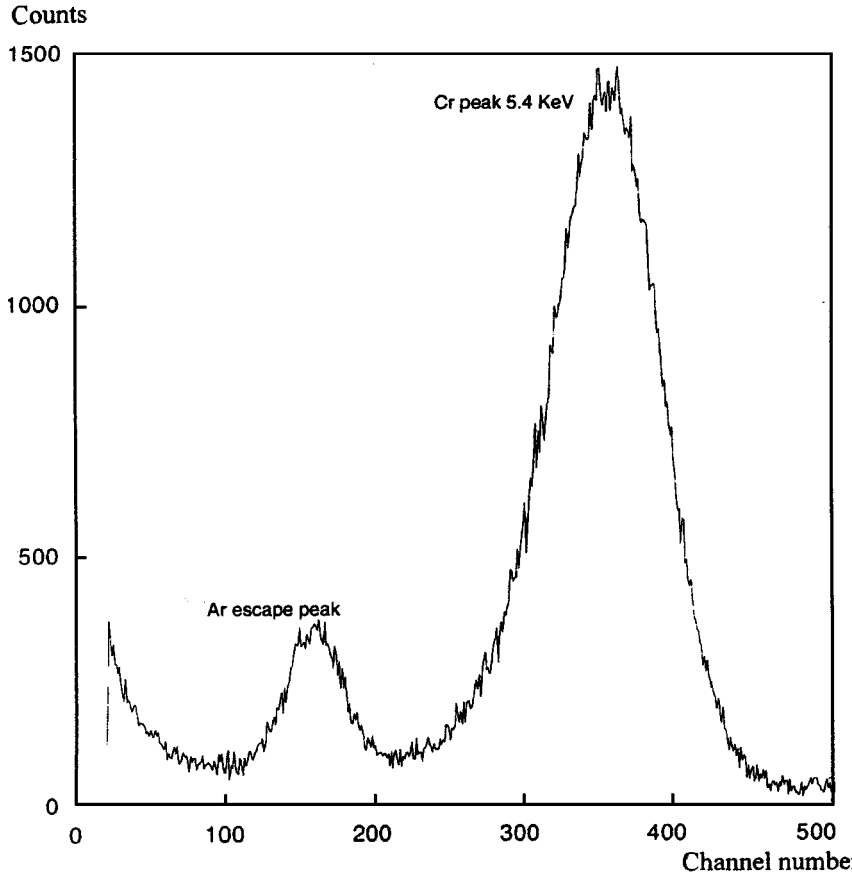

Figure 32 Example of the energy spectrum obtained for 5.4-keV X-rays with the compteur à trous. The resolution is 26% fwhm.

lower region; the GEM foil acts as a charge preamplifier, preserving the original ionization pattern to a large extent. The gain is a property of the GEM structure and is only mildly affected by the external fields, considerably relaxing the mechanical requirements. The GEM manufacturing method, developed at CERN, is a refinement of the double-side printed circuit technology. The metal-clad polymer (kapton) is engraved on both sides with the desired hole pattern; controlled immersion in a kapton-specific solvent opens the channels in the insulator.

The early measurements and the first application of the technology have been accomplished by combining the GEM amplifier with a standard MSGC (178–180). Figure 35 shows the gain characteristics obtained with such a two-stage detector. The rightmost curve corresponds to the characteristics of the MSGC alone; the others are obtained by progressively increasing the voltage across the

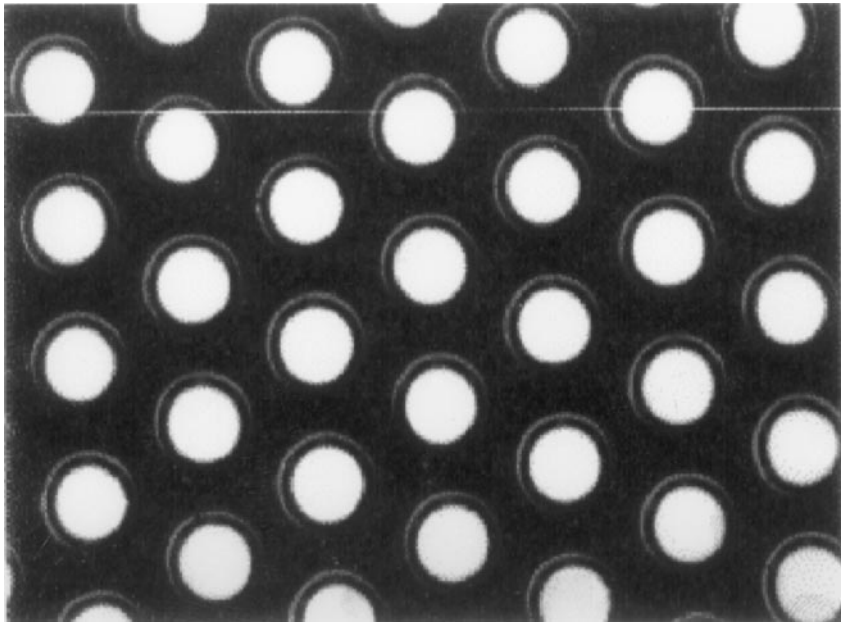

Figure 33 Close view of the hole structure in the gas electron multiplier. With chemical processing, a regular pattern of holes, typically 70 μm in diameter, is obtained on a thin, metal-coated polymer foil.

GEM foil. The cascaded device permits much higher gains, or, for a given required gain, permits operation of both the MSGC and the GEM at much lower voltages. Extensive tests under high flux and strongly ionizing particle irradiation have confirmed that the two-step detector is much more reliable. Two-step detectors have been adopted for the HERA-B tracker, which was originally based on large MSGC plates only.

The maximum gain achievable with the GEM electrode depends on the thickness of the polymeric support, the diameter of the holes, the gas mixture, and the applied voltages. Systematic research efforts have enabled GEM devices to achieve proportional gains up to 10^4, suitable for direct detection of ionization on simple charge-collecting printed circuit board (PCB) electrodes. Optimum performance is obtained with 50-μm-thick polymer foils, hole diameters of 50–100 μm, and a pitch of 100–200 μm. Figure 36 shows examples of gain measured with a single GEM in convenient, nonflammable mixtures of argon and carbon dioxide. Cascading two amplifying elements in a double GEM can produce gains well above 10^5 (Figure 37) (181–183). Systematic measurements with the structures show the relation between detected current and applied fields. As an example, Figure 38 shows the signal current, detected on the PCB strips, increasing almost linearly

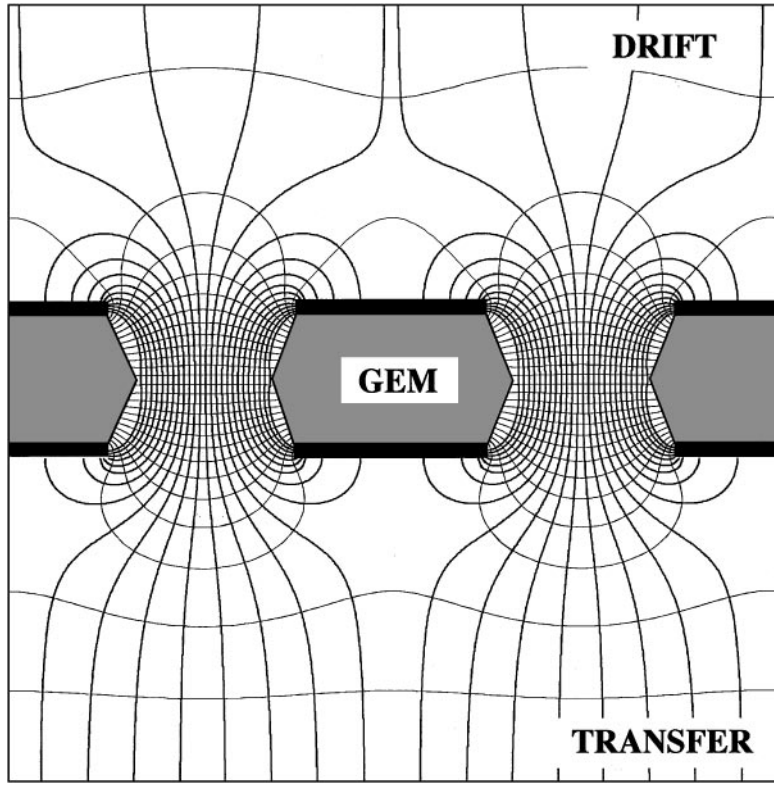

Figure 34 Electric field and equipotentials lines in the gas electron multiplier.

with the transfer field; the balance is collected by the lower GEM electrode (183). The large increase of charge at the highest fields corresponds to the onset of charge multiplication in the transfer gap. The current caused by positive ions is divided between the top GEM and the drift electrodes; its constancy demonstrates that the true gain is unaffected by the value of the transfer field. Similar measurements provide the effect of the drift field in the collection efficiency, or transparency.

Single and double GEM detectors with PCB readout have been extensively tested in the laboratory and in particle beams (184). Figure 39 shows the large efficiency plateau and the position resolution as a function of voltage obtained with a double GEM device.

In this mode of operation, the signal detected on the strips is entirely due to the electrons collection, without a slow ion tail, and is typically a few tens of nanoseconds wide for a 1-mm-wide gap. The method can be extended to obtain a projective two-dimensional readout, using double-level thin polymer foil with pads or strips interconnected in various patterns (see Figure 40) as pick-up electrodes (185). Both readout electrodes are kept at ground potential, giving the double GEM a

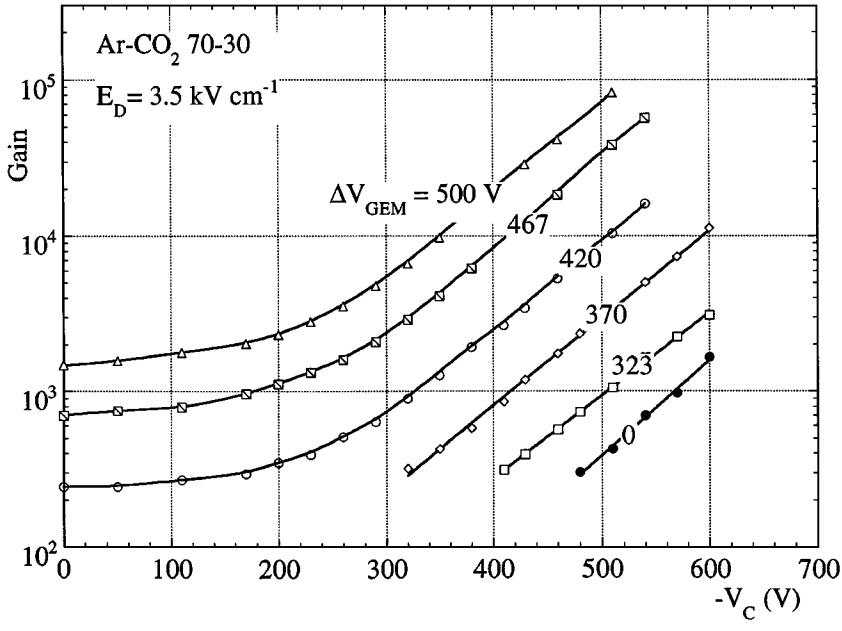

Figure 35 Gain curves measured, as a function of the cathode strips voltage V_C, in a two-stage detector consisting of a microstrip plate preceded by a gas electron multiplier (GEM). ΔV_{GEM} is the voltage applied between the two GEM electrodes.

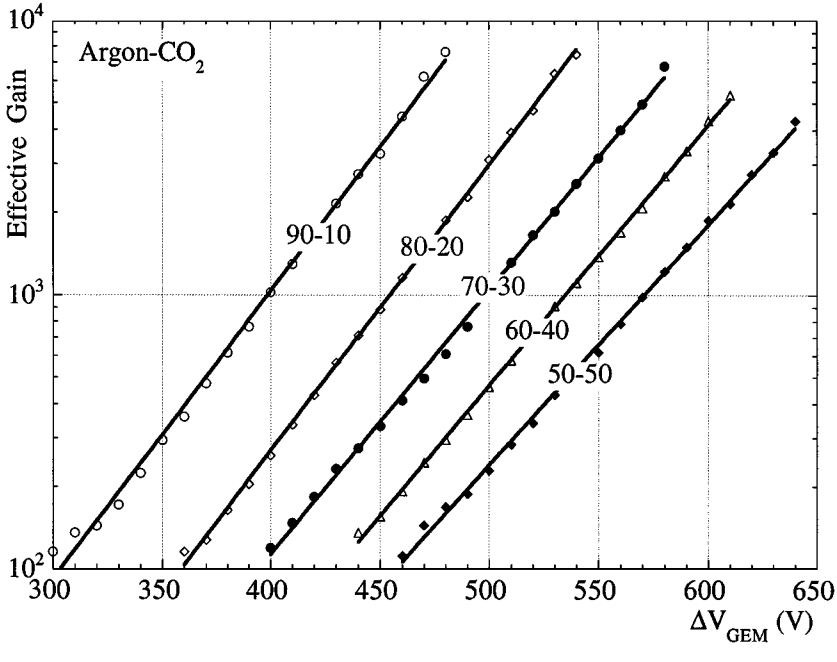

Figure 36 Effective gain curves measured with the single GEM+PCB (gas electron multiplier plus printed circuit board) detector in various argon-CO_2 mixtures. ΔV_{GEM} is the potential difference across the multiplier.

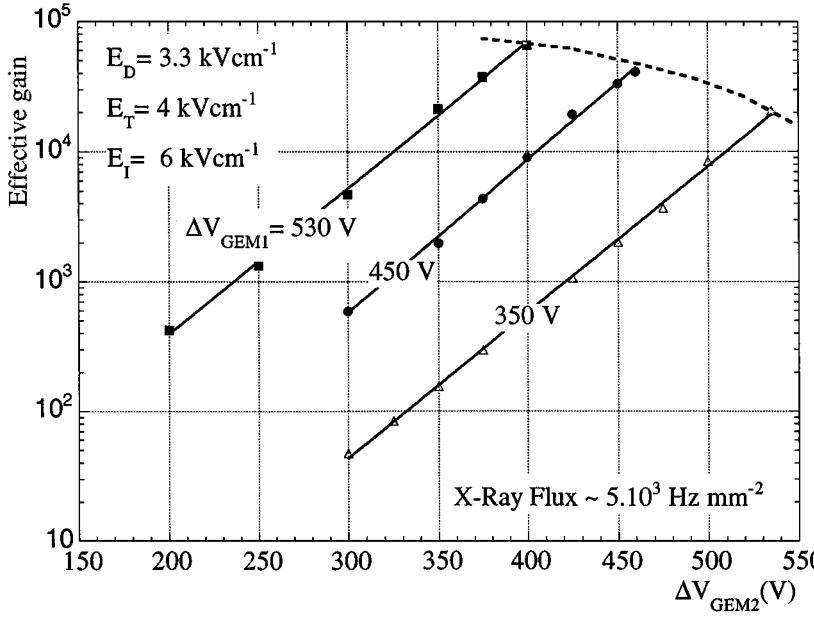

Figure 37 Gain curves measured with a double gas electron multiplier in cascade with printed circuit readout, as a function of voltages applied on one gas electron multiplier (GEM), ΔV_{GEM2}, for several values of the other GEM, ΔV_{GEM1}. E_D, E_T, and E_I are the fields in the drift, transfer, and induction region, respectively. The dashed line represents the discharge limit at an X-ray flux of $5 \cdot 10^5$ mm^{-2} s^{-1}. E_D and ΔV_{GEM} are the drift field and multiplying voltage.

substantial advantage over other two-dimensional devices, which require the use of high-voltage decoupling capacitors. The method of manufacturing the pick-up electrodes is based on the one developed for the GEM meshes. Two sets of parallel metal strips are engraved, using conventional printed-circuit technology, on the two sides of a thin kapton sheet. After gluing the foil on a thin insulating support, the polymer in the interstices between the upper strips is removed with a solvent, opening the bottom layer to charge collection. Very good charge correlation between the two projections and position accuracy of around 100 μm have been demonstrated. The signal induced on the lower GEM electrode can be used for triggering purposes, as shown in Figure 40. Figure 41 (see color insert) is a transmission radiography of the foot of a micromammal, realized with the described apparatus and using an 8-keV X-ray generator as radiation source. The image area is 9×7 mm^2, and the quality of the image demonstrates the good resolution and low noise of the system. For particle tracking, the good charge correlation between the two projections represents a powerful tool for unambiguous reconstruction of multiple events.

Like other micropattern devices, the GEM multipliers experience an increasing discharge rate under exposure to high radiation flux and highly ionizing tracks

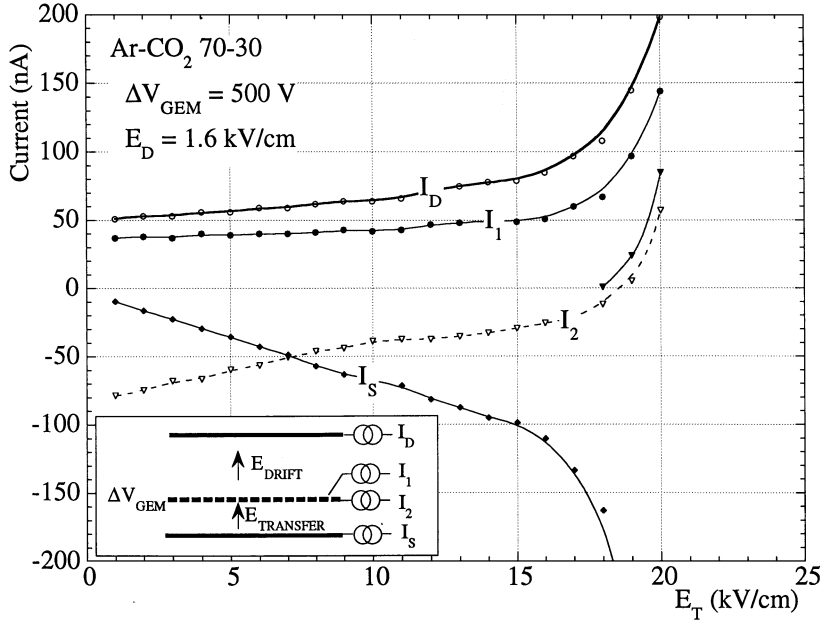

Figure 38 Currents measured in the gas electron multiplier with printed circuit board detector under uniform irradiation, as a function of transfer field E_T.

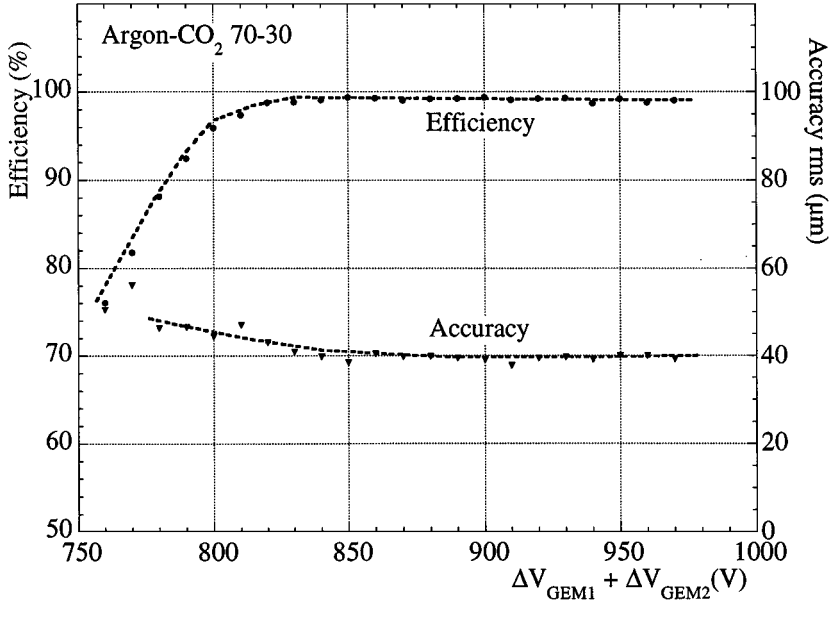

Figure 39 Efficiency and position accuracy for minimum ionizing particles measured with the double gas electron multiplier plus printed circuit board detector, as a function of total potential difference applied to the multipliers, $\Delta V_{GEM1} + \Delta V_{GEM2}$.

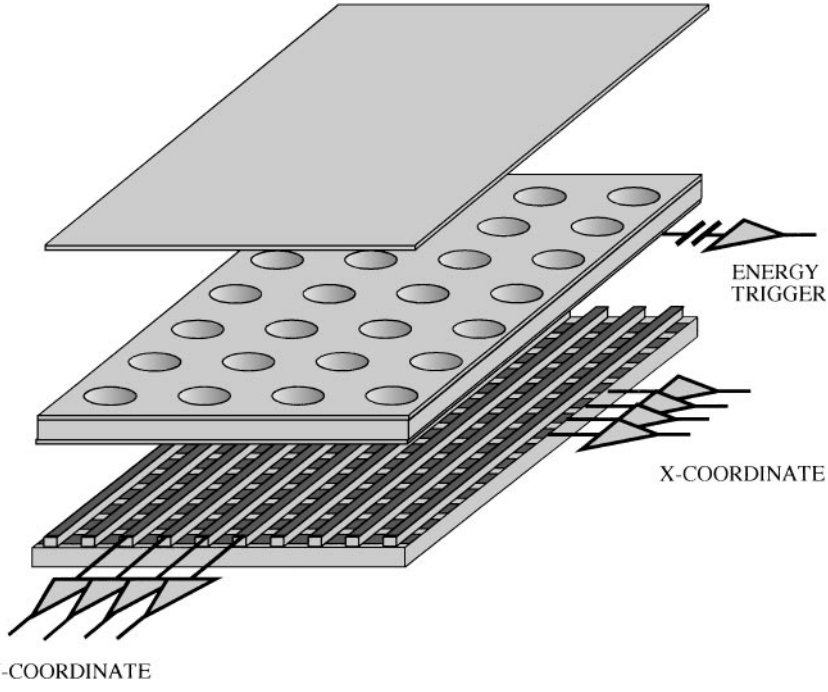

Figure 40 Schematics of a gas electron multiplier (GEM) detector with two-dimensional printed circuit board readout. Signals are read out on sets of perpendicular strips for the coordinate measurement, while the global signal detected on the lower GEM electrode serves the purpose of triggering and energy discrimination.

(120). Sharing the amplification process between two cascaded devices, however, shifts the maximum sustainable gain upward by at least an order of magnitude. The dashed contour in Figure 37 shows the upper boundary in the effective gain at the highest irradiation rate ($5\ 10^5$ Hz mm^{-2}); a value well above 10^4 is possible. Exposure to an internal alpha source produces a similar result. The tendency to withstand larger amounts of charge when the second multiplier operates at lower potential supports the presumption that the discharge limit depends on voltage (120). The low-field separation between multipliers is crucial, probably because it suppresses photon- and ion-mediated feedback mechanisms; its fundamental role has been confirmed by observed failures of detectors that directly combine two elements in contact.

The operation of GEM detectors has been studied in a wide range of conditions and gas fillings, for the detection of charged particles and X-rays (179, 186, 187) and of single photoelectrons, in view of possible applications in ring-imaging counters and large-area visible light imagers (188–190). A unique feature of the GEM structure is that, with an appropriate choice of the fields and geometry,

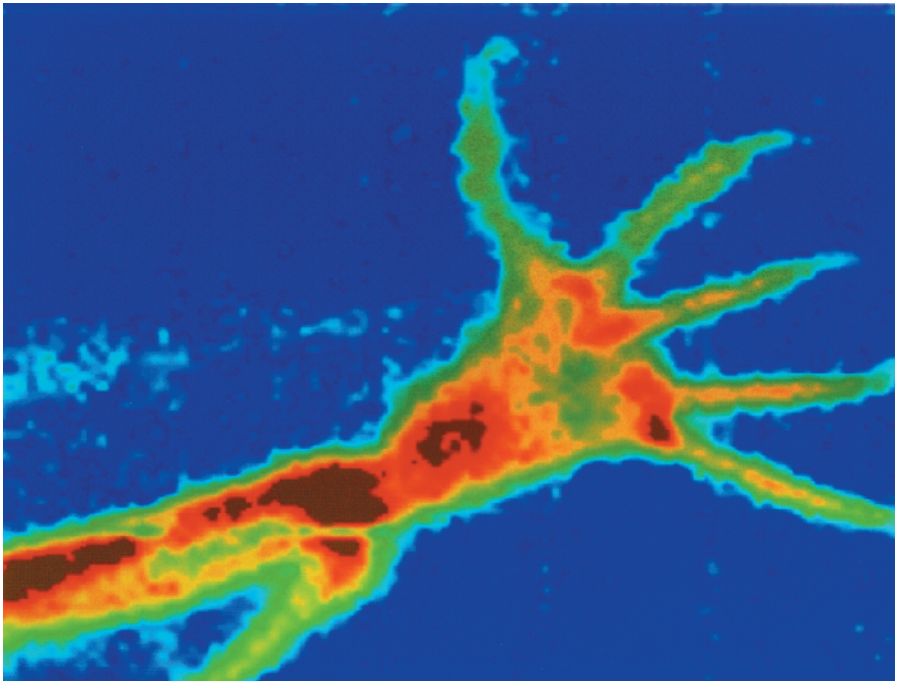

Figure 41 Example of the two-dimensional imaging capability of the gas electron multiplier detector: absorption radiography of a micromammal foot. The image size is $9 \times 7\ \mathrm{mm}^2$.

both photon and ion feedback are considerably suppressed from underlying structures into the sensitive volume. This characteristic suggests that GEM electrodes would be useful in devices intended to detect single electrons emitted by an internal photocathode. Promising preliminary work in this direction has been already reported in detectors operated at low pressures (187, 189). The recent observation of high gains in pure argon with single and multiple GEM structures also supports the possibility of implementing bialkali semitransparent photocathodes in a gas device (186, 188).

SUMMARY AND CONCLUSIONS

In the ten years since the introduction of the microstrip chamber, an amazingly large number of studies have aimed to understand the new detectors better and to improve their performance. Confronted by the instability problems inherent in the use of insulating supports, research has concentrated on the development of controlled resistivity substrates; thin coatings of diamond-like carbon and electron-conducting glass appear to be a reliable solution. Geometry, operating gases, and metals used for the strips have also been the subject of extensive studies and optimization efforts. Although successful in experimental setups requiring moderate proportional gains, MSGCs turned out to be prone to irreversible damage under harsher experimental conditions. The appearance of discharges on exposure to highly ionizing tracks has raised serious doubts about the reliability of large MSGC arrays of conventional design. Several techniques have been proposed to circumvent the problem, from passivation of the cathode strips edges (to prevent the propagation of discharges) to innovative designs of the micropattern structure, as in the microgap, microdot, and small-gap chambers. Although potentially far-reaching, these solutions require sophisticated, multimask processing only available in the microelectronics industry, in contrast to the simple photolithographic methods used to manufacture the standard MSGCs.

Several new micropattern detector concepts promise to increase reliability while preserving or even improving performance. These new detectors include the CAT, the micromegas, and the GEM. They all lack fragile thin anodes, achieving gain by avalanche multiplication along an extended high-field region. Manufactured with conventional albeit innovative technologies, the new devices are cheaper than microstrip devices and are free of their size limitations. The GEM has the unique feature of permitting the preamplification and transfer of charge, essentially preserving the ionization pattern, into a second element of amplification. Sharing the required gain between two or more cascaded amplifiers, each operated at a voltage well below the discharge limit, appears to be a sound solution to the problems common to all single-stage micropattern detectors.

A hundred years after the invention of the proportional counter, and thirty years after the multiwire chamber, the development of high-performance micropattern devices remains a challenging subject of research.

LITERATURE CITED

1. Charpak G, et al. *Nucl. Instrum. Methods* 62:262 (1968)
2. Sauli F. CERN 77–09 (1977)
3. Sauli F. In *Techniques and Concepts of High-Energy Physics*, ed. T Ferbel, pp. 301–50. New York: Plenum (1983)
4. Charpak G, Sauli F. *Annu. Rev. Nucl. Part. Sci.* 34:285–349 (1984)
5. Blum W, Rolandi G. *Particle Detection with Drift Chambers.* Berlin: Springer-Verlag (1993)
6. Grupen C. *Particle Detectors.* Cambridge, UK: Cambridge Univ. Press (1996)
7. Sauli F. *Nucl. Instrum. Methods* A419:189 (1998)
8. Sauli F. *Nucl. Instrum. Methods* A323:1 (1992)
9. Sauli *F. Rad. Protection Dosimetry* 61:29 (1995)
10. Neumann MJ, Nunamaker TA. *IEEE Trans. Nucl. Sci.* NS-17:43 (1970)
11. Christophel E, Dracos M. *Nucl. Instrum. Methods* A398:195 (1997)
12. Oed A. *Nucl. Instrum. Methods* A263:351 (1988)
13. Bartol F, et al. *J. Phys. III France* 6:337 (1996)
14. Giomataris I, et al. *Nucl. Instrum. Methods* A376:29 (1996)
15. Biagi SF, Jones TJ. *Nucl. Instrum. Methods* A361:72 (1995)
16. Sauli F. *Nucl. Instrum. Methods* A386:531 (1997)
17. Price W. *Nuclear Radiation Detectors.* New York: McGraw-Hill (1958)
18. Christophorou LG. *Atomic and Molecular Radiation Physics.* New York: Wiley (1971)
19. Knoll G. *Radiation Detection and Measurement.* New York: Wiley (1989)
20. Delaney CFG, Finch EC. *Particle Detectors: Physical Principles and Applications.* Oxford, UK: Clarendon (1992)
21. Budtz-Jørgensen C. *Rev. Sci. Instrum.* 63: 648 (1992)
22. Bouclier R, et al. *Nucl. Instrum. Methods* A323:240 (1992)
23. Bateman JE, Connolly JF. RAL-92–085 (1992)
24. Oed A. *Nucl. Instrum. Methods* A367:34 (1995)
25. Sauli F. CERN/DRDC/93–34 (1993)
26. Sauli F. *Nucl. Phys.* B61:236 (1998)
27. Della Mea G, Sauli F, eds. *Proc. Int. Workshop Micro-Strip Gas Chambers, Legnaro, 1994, Progetto, Padova, Italy* (1995)
28. Contardo D, Sauli F, eds. *Proc. Int. Workshop Micro-Strip Gas Chambers, Lyon, 1995.* Lyon, France: Medcom (1996)
29. Florent JJ, et al. *Nucl. Instrum. Methods* A329:125 (1993)
30. Bellazzini R, Spezziga MA. *Riv. Nuovo Cim.* 17:1 (1994)
31. Biagi SF. *Nucl. Instrum. Methods* A283: 716 (1989)
32. Veenhof R. *Nucl. Instrum. Methods* A419: 726 (1998)
33. Angelini F, et al. *Nucl. Instrum. Methods* A382:461 (1996)
34. Bateman JE, et al. RAL-95–038 (1995)
35. Bouclier R, et al. *Nucl. Instrum. Methods* 367:168 (1995)
36. Fang R, et al. *Nucl. Instrum. Methods* A378:439 (1996)
37. Cicognani G, et al. *Nucl. Instrum. Methods* A392:115 (1997)
38. Frolov AR, et al. *Nucl. Instrum. Methods* A307:497 (1991)
39. Minakov GD, et al. *Nucl. Instrum. Methods* A326:566 (1993)
40. Bouclier R, et al. *Nucl. Instrum. Methods* A332:100 (1993)
41. Bouclier R, et al. *IEEE Trans. Nucl. Sci.* NS-41:821 (1994)
42. Bateman JE, et al. In *Proc. MSGC Workshop, Legnaro*, p. 22 (1994)

43. Pestov YN, Shekhtman LI. *Nucl. Instrum. Methods* A338:368 (1994)
44. Gerndt EKE, et al. *Nucl. Instrum. Methods* A388:42 (1997)
45. Angelini F, et al. *Nucl. Instrum. Methods* A314:450 (1992)
46. Pallarès A, et al. CRN 95–14 (1995)
47. Della Mea G, et al. *J. Am. Ceramic Soc.* 76:2930 (1993)
48. Della Mea G, et al. *Thin Solid Films* 241:25 (1994)
49. Bouclier R, et al. In *Proc. MSGC Workshop, Legnaro*, p. 39 (1994)
50. Gong WG, et al. *Nucl. Instrum. Methods* A360:30 (1994)
51. Bateman JE, et al. RAL-TR-95–032 (1995)
52. Bouclier R, et al. *Nucl. Instrum. Methods* A369:328 (1996)
53. Boimska B, et al. *Nucl. Instrum. Methods* A400:9 (1997)
54. Boimska B, et al. *Nucl. Instrum. Methods* A404:57 (1997)
55. Barr A, et al. *Nucl. Phys.* B61:315 (1996)
56. Zeuner T. *Nucl. Instrum. Methods* A392: 105 (1997)
57. Savard P, et al. *Nucl. Instrum. Methods* A337:125 (1993)
58. Bagulya AV, et al. In *Proc. MSGC Workshop, Lyon*, p. 243 (1995)
59. Cho HS, et al. *Nucl. Instrum. Methods* A40181 (1997)
60. Buzulutskov A, et al. *Nucl. Instrum. Methods* A409:33 (1998)
61. Salomon M, et al. TRI-PP 94–24 (1994)
62. Brons S, et al. *Nucl. Instrum. Methods* A342:411 (1994)
63. Bouclier R, et al. *IEEE Trans. Nucl. Sci.* NS-43:1220 (1996)
64. Stahl H, et al. *Nucl. Instrum. Methods* A297:95 (1990)
65. Schmidt S, et al. *Nucl. Instrum. Methods* A337:382 (1994)
66. Dixit M, et al. *Nucl. Instrum. Methods* A348:365 (1994)
67. Salomon M, et al. *IEEE Trans. Nucl. Sci.* NS-41:817 (1994)
68. Salomon M, et al. *IEEE Trans. Nucl. Sci.* NS-43:1157 (1996)
69. Bouclier R, et al. *Nucl. Instrum. Methods* A365:65 (1995)
70. Beckers T, et al. *Nucl. Instrum. Methods* A346:95 (1994)
71. Bateman JE, Connolly JF. RAL-94–114 (1994)
72. Brom JM, et al. CRN 95–14 (1995)
73. Bouhali O, et al. *Nucl. Instrum. Methods* A378:432 (1996)
74. Jelen K, et al. *Nucl. Instrum. Methods* A392:80 (1997)
75. van Hunen JJ. *Nucl. Instrum. Methods* A 409:95 (1998)
76. Bohm J, et al. *Nucl. Instrum. Methods* A360:34 (1995)
77. Kiourkos S, et al. *Nucl. Instrum. Methods* A348:351 (1994)
78. Snow S, et al. In *Proc. MSGC Workshop, Lyon*, p. 127 (1995)
79. Pooth O, *Nucl. Instrum. Methods* A419: 375 (1998)
80. Bouhali O, et al. In *Proc. MSGC Workshop, Lyon*, p. 101 (1995)
81. Barthe S, et al. In *Proc. MSGC Workshop, Lyon* p. 107 (1995)
82. Duerdoth I, et al. *Nucl. Instrum. Methods* A348:356 (1994)
83. Mack V, et al. *Nucl. Instrum. Methods* A367:173 (1995)
84. Angelini F, et al. LHC Workshop, Aachen 4–9 October 1990. CERN 90-10 (1990)
85. Geijsberts M, et al. *Nucl. Instrum. Methods* A313:377 (1992)
86. Dixit MS, et al. In *Proc. MSGC Workshop, Legnaro*, p. 138 (1994)
87. Bouhali O, et al. IISN0379–301X (1996)
88. Amos N, et al. *Nucl. Instrum. Methods* A384:342 (1997)
89. Gómez F, et al. *Nucl. Instrum. Methods* A384:351 (1997)
90. Barr A, et al. *Nucl. Instrum. Methods* A392:99 (1997)
91. Barr A, et al. *Nucl. Instrum. Methods* A403:31 (1998)

92. Abbaneo D, et al. *Nucl. Instrum. Methods* A409:37 (1998)
93. Bachman S, et al. *Nucl. Instrum. Methods* A409:6 (1998)
94. Albert E, et al. *Nucl. Instrum. Methods* A409:70 (1998)
95. Ballintijn MK, et al. NIKHEF 95–002 (1995)
96. Henkes T, et al. In *Proc. MSGC Workshop, Lyon*, p. 143 (1995)
97. de Groot N, et al. In *Proc. MSGC Workshop, Lyon*, p. 137 (1995)
98. Blouw J, et al. In *Proc. MSGC Workshop, Lyon*, p. 143 (1995)
99. Landry M, et al. *Nucl. Instrum. Methods* A421:31 (1998)
100. Hall G. In *Proc. MSGC Workshop, Lyon*, p. 165 (1994)
101. Bouclier R, et al. In *Proc. MSGC Workshop, Legnaro*, p. 79 (1994)
102. Clergeau J-F, et al. *Nucl. Instrum. Methods* A392:109 (1997)
103. Schmitz J. *Nucl. Instrum. Methods* A323: 638 (1992)
104. Angelini F, et al. *Nucl. Phys.* A23:254 (1991)
105. van den Berg FD, et al. *Nucl. Instrum. Methods* A349:438 (1994)
106. Abbaneo D, et al. CERN-CMS CR 1998/ 012 (1998)
107. Baiboussinov B, et al. CMS TN/95–201 (1995)
108. Cicognani G, et al. *IEEE Trans. Nucl. Sci.* NS-45:249 (1998)
109. Vellettaz N, et al. *Nucl. Instrum. Methods* A392:73 (1997)
110. Vellettaz N, et al. In *Proc. MSGC Workshop, Lyon*, p. 73 (1995)
111. Capeáns M, et al. *Nucl. Phys.* B61:17 (1998)
112. Angelini F, et al. *Nucl. Instrum. Methods* A283:755 (1989)
113. Angelini F, et al. *Nucl. Instrum. Methods* A323:229 (1992)
114. Nagae T, et al. *Nucl. Instrum. Methods* A323:236 (1992)
115. Tanimori T, et al. *Nucl. Instrum. Methods* A381:280 (1996)
116. Ochi A, et al. *Nucl. Instrum. Methods* A392:124 (1997)
117. Peskov V, et al. *Nucl. Instrum. Methods* A397:243 (1997)
118. Peskov V, et al. *IEEE Trans. Nucl. Sci.* NS-45:244 (1998)
119. Schmidt B. *Nucl. Instrum. Methods* A419:230 (1998)
120. Bressan A, et al. *Nucl. Instrum. Methods* A424:321 (1998)
121. Keller S, et al. *Nucl. Instrum. Methods* A419:382 (1998)
122. Fonte P, et al. *Nucl. Instrum. Methods* A419:405 (1998)
123. Cho HS, et al. *IEEE Trans. Nucl. Sci.* NS-44:635 (1997)
124. Cho HS, et al. *IEEE Trans. Nucl. Sci.* NS-45:280 (1998)
125. Schmidt B. In *Proc. Workshop New Detectors, Erice 1997*, ed. T Ypsilani, p. 270. Singapore: World Sci. (1999)
126. Bellazzini R, et al. *Nucl. Instrum. Methods* A398:426 (1998)
127. Va'vra J. In *Proc. Workshop Radiat. Damage to Wire Chambers, Jan 16–17, 1986*, ed. J Kadyk, p. 263 (1986). LBL-21170
128. Va'vra J. *Nucl. Instrum. Methods* A323: 34 (1992)
129. Bouclier R, et al. *Nucl. Instrum. Methods* A350:464 (1994)
130. Bouclier R, et al. *Nucl. Instrum. Methods* A381:289 (1996)
131. Bouclier R, et al. In *Proc. MSGC Workshop, Legnaro*, p. 48 (1994)
132. Duerdoth IP, et al. *Nucl. Instrum. Methods* A392:127 (1997)
133. van den Berg FD, et al. *Nucl. Instrum. Methods* A392:94 (1997)
134. Schefer J, et al. In *Proc. MSGC Workshop, Legnaro*, p. 173 (1994)
135. Ramsey BD, et al. In *Proc. SPIE 1994 Int. Symp. Optical Appl. Sci. Eng., San Diego*, p. 31 (1994)
136. Dixit MS, et al. *IEEE Trans. Instrum. Meas.* IMTC/97 (1997)
137. Zhukov V, et al. *Nucl. Instrum. Methods* A392:83 (1997)

138. Gebauer B, et al. *Nucl. Instrum. Methods* A392:68 (1997)
139. Gebauer B, et al. *Nucl. Instrum. Methods* A409:56 (1998)
140. Breskin A, et al. *Nucl. Instrum. Methods* A345:205 (1994)
141. Zeitelhack K, et al. In *Proc. MSGC Workshop, Lyon*, p. 53 (1995)
142. Anderson DF, et al. *Nucl. Phys.* B44:213 (1995)
143. Eckardt V, et al. In *Proc. MSGC Workshop, Legnaro*, p. 184 (1994)
144. Frankenfeld U, Sann H. *Proc. MSGC Workshop, Lyon*, p. 85 (1995)
145. Baru SE, et al. In *Proc. MSGC Workshop, Lyon*, p. 27 (1995)
146. Geltenbort P, Oed A. In *Proc. Eur. Workshop X-ray Detect. Synchrotron Radiat. Sources, Assois Sept. 30–Oct. 4, 1991*, ed. AH Walenta, p. 107. (1999)
147. Geltenbort P, Oed A. In *Proc. SPIE 1992 Int. Symp. Optical Appl. Sci. Eng., San Diego* (1992)
148. Akimov D, et al. In *Proc. MSGC Workshop, Legnaro*, p. 215 (1994)
149. Policarpo AJP, et al. *Nucl. Instrum. Methods* A365:568 (1995)
150. Angelini F, et al. *Nucl. Instrum. Methods* A335:69 (1993)
151. Angelini F, et al. *Nucl. Instrum. Methods* A349:273 (1995)
152. Angelini A, et al. In *Proc. MSGC Workshop, Lyon*, p. 307 (1995)
153. van den Berg FD, et al. *Nucl. Instrum. Methods* A409:90 (1998)
154. Biagi SF, et al. *Nucl. Instrum. Methods* A392:131 (1997)
155. Angelini F, et al. In *Proc. MSGC Workshop, Lyon*, p. 91 (1995)
156. Bellazzini R, et al. *Nucl. Instrum. Methods* A409:14 (1998)
157. Cho HS, et al. *IEEE Trans. Nucl. Sci.* NS-44:747 (1997)
158. Fraga FAF, et al. *Nucl. Instrum. Methods* A392:135 (1997)
159. Fraga FAF, et al. *Nucl. Instrum. Methods* A419:460 (1998)
160. Clergeau J-F, et al. *Nucl. Instrum. Methods* A392:140 (1997)
161. Chorowicz V, et al. *Nucl. Instrum. Methods* A401:238 (1997)
162. Biagi SF, et al. *Nucl. Instrum. Methods* A371:12 (1995)
163. Biagi S, et al. *Nucl. Instrum. Methods* A 419:438 (1998)
164. Biagi SF, et al. *Nucl. Instrum. Methods* 61B:311 (1998)
165. Breskin A, et al. *Nucl. Instrum. Methods* A394:21 (1997)
166. Fonte P, et al. *Nucl. Instrum. Methods* A305:91 (1991)
167. Fonte P. *IEEE Trans. Nucl. Sci.* NS-43:2135 (1996)
168. Ivaniouchenkov I, et al. *IEEE Trans. Nucl. Sci.* NS-45:258 (1998)
169. Giomataris Y. *Nucl. Instrum. Methods* A 419:239 (1998)
170. Barouch G, et al. *Nucl. Instrum. Methods* A423:32 (1999)
171. Cussonneau JP, et al. *Nucl. Instrum. Methods* A419:452 (1998)
172. Schmitz J. NIKHEF-H/91–14 (1991)
173. Jeavons A, et al. *Nucl. Instrum. Methods* 176:89 (1980)
174. Sarvestrani A, et al. *Nucl. Instrum. Methods* A419:444 (1998)
175. Sarvestani A, et al. In *Proc. MSGC Workshop, Lyon*, p. 45 (1995)
176. Charpak G, Sauli F. *Phys. Lett.* B78:523 (1978)
177. Adams M, et al. *Nucl. Instrum. Methods* 217:237 (1983)
178. Bouclier R, et al. *Nucl. Instrum. Methods* A396:50 (1997)
179. Beaumont W, et al. *Nucl. Instrum. Methods* A419:394 (1998)
180. Benhammou Y, et al. *Nucl. Instrum. Methods* A419:400 (1998)
181. Benlloch J, et al. *IEEE Trans. Nucl. Sci.* NS-45:234 (1998)
182. Büttner C, et al. *Nucl. Instrum. Methods* A409:79 (1998)
183. Benlloch J, et al. *Nucl. Instrum. Methods* A419:410 (1998)

184. Bressan A, et al. *Nucl. Instrum. Methods* A:425:262 (1999)
185. Bressan A, et al. *Nucl. Instrum. Methods* A425:254 (1999)
186. Bressan A, et al. *Nucl. Instrum. Methods* A423:119 (1999)
187. Chechik R, et al. *Nucl. Instrum. Methods* A:419:423 (1999)
188. Buzulutskov A, et al. Presented at Int. Workshop on Ring Imaging Cherenkov Detectors RICH38, Ein Gedi, Israel, Nov. 15–20, 1998
189. Garty G, et al. Presented at Int. Workshop on Ring Imaging Cherenkov Detectors RICH38, Ein Gedi, Israel, Nov. 15–20, 1998
190. Va'vra J, et al. Presented at Int. Workshop on Ring Imaging Cherenkov Detectors RICH38, Ein Gedi, Israel, Nov. 15–20, 1998

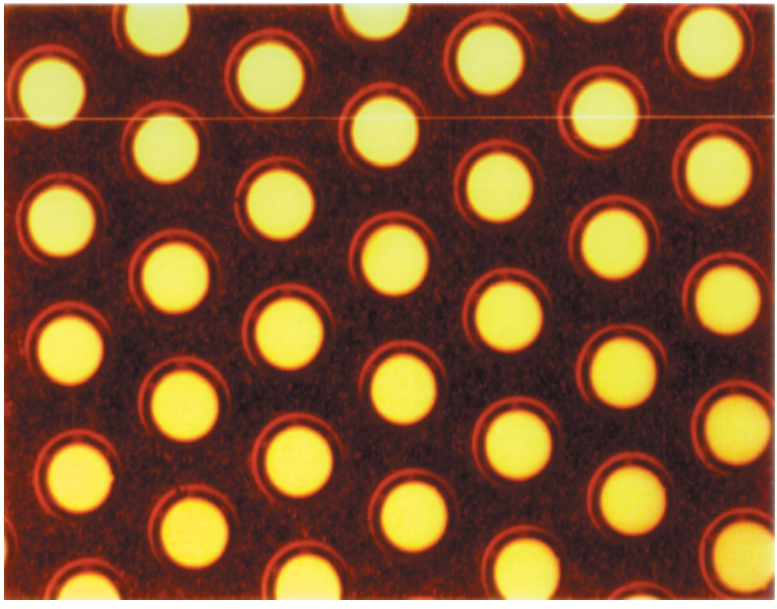

Figure 33 Close view of the hole structure in the gas electron multiplier. With chemical processing, a regular pattern of holes, typically 70 μm in diameter, is obtained on a thin, metal-coated polymer foil.

Annual Review of Nuclear and Particle Science
Volume 49, 1999

CONTENTS

SNAPSHOTS OF A PHYSICIST'S LIFE, *J. David Jackson* 1
RECENT PROGRESS IN BARYOGENESIS, *Antonio Riotto, Mark Trodden* 35
THE COSMIC MICROWAVE BACKGROUND AND PARTICLE PHYSICS, *Marc Kamionkowski, Arthur Kosowsky* 77
MEASUREMENT OF SMALL ELECTRON-BEAM SPOTS, *Peter Tenenbaum, Tsumoru Shintake* 125
PARTICLE PHYSICS FROM STARS, *Georg G. Raffelt* 163
HIGH-ENERGY HADRON-INDUCED DILEPTON PRODUCTION FROM NUCLEONS AND NUCLEI, *P. L. McGaughey, J. M. Moss, J. C. Peng* 217
CHARMONIUM SUPPRESSION IN HEAVY-ION COLLISIONS, *C. Gerschel, J. Hüfner* 255
SPIN STRUCTURE FUNCTIONS, *E. W. Hughes, R. Voss* 303
MICROPATTERN GASEOUS DETECTORS, *Fabio Sauli, Archana Sharma* 341
LEPTOQUARK SEARCHES AT HERA AND THE TEVATRON, *Darin E. Acosta, Susan K. Blessing* 389
DIRECT MEASUREMENT OF THE TOP QUARK MASS, *Kirsten Tollefson, Erich W. Varnes* 435
NEUTRINO MASS AND OSCILLATION, *Peter Fisher, Boris Kayser, Kevin S. McFarland* 481
TWO-PARTICLE CORRELATIONS IN RELATIVISTIC HEAVY-ION COLLISIONS, *Ulrich Heinz, Barbara V. Jacak* 529
COLLECTIVE FLOW IN HEAVY-ION COLLISIONS, *Norbert Herrmann, Johannes P. Wessels, Thomas Wienold* 581
INCLUSIVE JET AND DIJET PRODUCTION AT THE TEVATRON, *Gerald C. Blazey, Brenna L. Flaugher* 633